

UC Davis

UC Davis Previously Published Works

Title

Consensus statement on current and emerging methods for the diagnosis and evaluation of cerebrovascular disease

Permalink

<https://escholarship.org/uc/item/8jn6j92h>

Journal

Cerebrovascular and Brain Metabolism Reviews, 38(9)

ISSN

1040-8827

Authors

Donahue, Manus J
Achten, Eric
Cogswell, Petrice M
et al.

Publication Date

2018-09-01

DOI

10.1177/0271678x17721830

Peer reviewed

Consensus statement on current and emerging methods for the diagnosis and evaluation of cerebrovascular disease

Manus J Donahue^{1,2,3,4}, Eric Achten⁵, Petrice M Cogswell¹, Frank-Erik De Leeuw⁶, Colin P Derdeyn⁷, Rick M Dijkhuizen⁸, Audrey P Fan⁹, Rashid Ghaznawi¹⁰, Jeremy J Heit¹¹, M Arfan Ikram^{12,13}, Peter Jezzard¹⁴, Lori C Jordan¹⁵, Eric Jouvent¹⁶, Linda Knutsson^{17,18}, Richard Leigh¹⁹, David S Liebeskind²⁰, Weili Lin²¹, Thomas W Okell¹⁴, Adnan I Qureshi²², Charlotte J Stagg²³, Matthias JP van Osch²⁴, Peter CM van Zijl^{17,25}, Jennifer M Watchmaker¹, Max Wintermark¹¹, Ona Wu^{26,27}, Greg Zaharchuk¹¹, Jinyuan Zhou^{17,25} and Jeroen Hendrikse¹⁰

Abstract

Cerebrovascular disease (CVD) remains a leading cause of death and the leading cause of adult disability in most developed countries. This work summarizes state-of-the-art, and possible future, diagnostic and evaluation approaches in multiple stages of CVD, including (i) visualization of sub-clinical disease processes, (ii) acute stroke theranostics, and (iii) characterization of post-stroke recovery mechanisms. Underlying pathophysiology as it relates to large vessel

¹Department of Radiology and Radiological Sciences, Vanderbilt University Medical Center, Nashville, TN, USA

²Department of Neurology, Vanderbilt University Medical Center, Nashville, TN, USA

³Department of Psychiatry, Vanderbilt University Medical Center, Nashville, TN, USA

⁴Department of Physics and Astronomy, Vanderbilt University, Nashville, TN, USA

⁵Department of Radiology and Nuclear Medicine, Universiteit Gent, Gent, Belgium

⁶Radboud University, Nijmegen Medical Center, Donders Institute Brain Cognition & Behaviour, Center for Neuroscience, Department of Neurology, Nijmegen, The Netherlands

⁷Department of Radiology and Neurology, University of Iowa, Iowa City, IA, USA

⁸Biomedical MR Imaging and Spectroscopy Group, Center for Image Sciences, University Medical Center Utrecht, Utrecht, The Netherlands

⁹Department of Radiology, Stanford University, Stanford, CA, USA

¹⁰Department of Radiology, University Medical Center Utrecht, Utrecht, The Netherlands

¹¹Department of Radiology, Neuroimaging and Neurointervention Division, Stanford University, CA, USA

¹²Department of Epidemiology, Erasmus MC, Rotterdam, The Netherlands

¹³Department of Radiology, Erasmus MC, Rotterdam, The Netherlands

¹⁴Nuffield Department of Clinical Neurosciences, University of Oxford, John Radcliffe Hospital, Oxford, UK

¹⁵Department of Pediatrics, Division of Pediatric Neurology, Vanderbilt University Medical Center, Nashville, TN, USA

¹⁶Department of Neurology, AP-HP, Lariboisière Hospital, Paris, France

¹⁷Department of Radiology and Radiological Science, Johns Hopkins University School of Medicine, Baltimore, MD, USA

¹⁸Department of Medical Radiation Physics, Lund University, Lund, Sweden

¹⁹National Institute of Neurological Disorders and Stroke, National Institutes of Health, Bethesda, MD, USA

²⁰Neurovascular Imaging Research Core, UCLA, Los Angeles, CA, USA

²¹Department of Biomedical Engineering, University of North Carolina at Chapel Hill, Chapel Hill, NC, USA

²²Department of Neurology, Zeenat Qureshi Stroke Institute, St. Cloud, MN, USA

²³Oxford Centre for Human Brain Activity, University of Oxford, Oxford, UK

²⁴Department of Radiology, Leiden Medical Center, Leiden, The Netherlands

²⁵F.M. Kirby Research Center for Functional Brain Imaging, Kennedy Krieger Institute, Baltimore, MD, USA

²⁶Athinoula A. Martinos Center for Biomedical Imaging, Department of Radiology, Massachusetts General Hospital, Charlestown, MA, USA

²⁷Department of Radiology, Harvard Medical School, Boston, MA, USA

Corresponding author:

Manus J Donahue, Radiology and Radiological Sciences, Vanderbilt University Medical Center, 1161 21st Ave South, Nashville, TN 37232, USA. Email: mj.donahue@vanderbilt.edu

steno-occlusive disease and the impact of this macrovascular disease on tissue-level viability, hemodynamics (cerebral blood flow, cerebral blood volume, and mean transit time), and metabolism (cerebral metabolic rate of oxygen consumption and pH) are also discussed in the context of emerging neuroimaging protocols with sensitivity to these factors. The overall purpose is to highlight advancements in stroke care and diagnostics and to provide a general overview of emerging research topics that have potential for reducing morbidity in multiple areas of CVD.

Keywords

Stroke, hemodynamics, metabolism, imaging, cerebrovascular disease

Received 17 March 2017; Revised 26 May 2017; Accepted 10 June 2017

Introduction

Stroke, defined as a severe interruption or reduction in blood supply to the brain, remains a leading cause of death, and the leading cause of adult disability, in most developed countries. Approximately 87% of strokes are ischemic, originating from an obstruction within a blood vessel, whereas the remainder are hemorrhagic, or caused by vessel rupture. Cerebrovascular disease (CVD) more broadly comprises conditions that affect the blood supply to the brain and can lead to overt stroke when severe or inadequately managed. Despite progress in acute stroke treatment, 20–30% of strokes result in death within one month and 70–80% result in significant long-term disability.^{1,2} These statistics highlight the need to both improve acute stroke theranostic procedures and address preventative and rehabilitative care comprehensively.

Stroke is often referred to as a cerebrovascular accident, but is associated with many well-defined lifestyle and vascular risk factors.³ As a result, the majority of strokes might be preventable with appropriate risk factor management and surveillance of cerebrovascular health. Neuroimaging is a critical component of patient care in most stages of CVD: from identification of stroke risk factors to stratifying acute and chronic stroke patients to the most effective revascularization and in some cases rehabilitation treatments.

Here, we outline current and emerging methods for understanding CVD in the settings of: (i) chronic CVD and stroke prevention, (ii) acute ischemic and hemorrhagic stroke, and (iii) stroke recovery. As lifestyle factors contributing to CVD have been characterized extensively,³ the focus of this work is to summarize major changes to tissue hemodynamics and metabolism that contribute to CVD and stroke risk, along with an overview of established clinical and emerging research tools for characterizing these parameters. The overall goal is to highlight advances in pathophysiological characterization of tissue in each of these stages of CVD, and to identify unmet clinical needs and relevant future directions.

Physiology of ischemia

Macrovascular and tissue-level changes in chronic ischemia

Human brain tissue consumes higher levels of glucose (cerebral metabolic rate of glucose, CMR_{Glc}) and oxygen (cerebral metabolic rate of oxygen consumption, CMR_{O_2}) compared with any other organ tissue.^{4–7} Furthermore, as anaerobic glycolysis provides insufficient energy to support metabolic demand, and the amount of oxygen stored in brain tissue is extremely small, the brain is dependent on the circulation for a continuous supply of energy substrate. Delivered oxygen is primarily used for oxidation of glucose and to a lesser extent for oxidases relevant to neurotransmitter synthesis and metabolism. As such the regulation of blood flow in the brain, the cerebral blood flow (CBF; ml blood/100 g tissue/minute), is crucial to maintaining O_2 delivery and is controlled by a variety of global vascular factors such as collateralization, as well as more local chemical factors, including autoregulatory vasodilatory effects arising from partial pressure of arterial CO_2 ($PaCO_2$) increases, partial pressure of arterial O_2 (PaO_2) decreases, and pH alterations. Table 1 summarizes ranges of these and related parameters for healthy and ischemic adult tissue. In health, these mechanisms ensure a comparatively high whole-brain CBF of 40–60 ml/100 g/min, which translates to 700–800 mL blood/min, or approximately 15% of cardiac output. If blood flow ceases entirely, consciousness is lost in approximately 10 s, just slightly longer than the time required to extract and consume oxygen from the blood.

Acute ischemic stroke (AIS) occurs when the CBF required to maintain normal tissue function reduces below necessary thresholds (18–25 ml/100 g/min in gray matter and two to three times lower in white matter) and arises during arterial steno-occlusion due to either a thrombosis (vessel obstruction from local mass) or embolism (obstruction due to mass traveling from elsewhere), where the mass is most often a blood clot or cholesterol plaque. In other cases, ischemia may be due to more systemic decreases in blood supply or

Table 1. Summary of many relevant physiological parameters for assessing tissue health in stroke.

Parameter	Description	Adult healthy range	Approximate pathological threshold in adult ischemia	Measurement tools	References
CBF	Rate of blood delivery to tissue (ml blood/100 g tissue/min)	35–60 ml/100 g tissue/min (gray matter) 17–28 ml/100 g tissue/min (white matter)	<20 ml/100 g tissue/min (gray matter) <10 ml/100 g tissue/min (white matter)	15O-water PET, CT perfusion, DSC MRI, ASL MRI	Leenders et al. ²¹⁸ Derdeyn et al. ¹¹
CBV	Volume of blood per volume of brain (ml blood/100 g tissue)	3.5–6.6 ml/100 g tissue (gray matter) 2.1–3.0 ml/100 g tissue (white matter)	>8.5 ml blood/100 g tissue (autoregulation; gray matter) >3.5 ml blood/100 g tissue (autoregulation; white matter, thresholds less established) <42% of contralateral (healthy) hemisphere CBV may predict parenchymal hematoma	15O-water PET, CT perfusion, DSC MRI	Leenders et al. ²¹⁸ Derdeyn et al. ¹¹ Mishra et al. ²¹⁹
OEF	Ratio of oxygen consumed to oxygen delivered (unitless)	0.35–0.44 (gray matter) 0.31–0.42 (white matter)	>0.50 (gray matter) >0.46 (white matter)	15O-water PET, SWI MRI, TRUST MRI	Leenders et al. ²¹⁸ Derdeyn et al. ¹¹
MTT	Mean time in seconds that red blood cells spend to traverse the capillary circulation (MTT = CBV/CBF)	3.8–6.6 s (gray matter) 4.6–7.4 s (white matter)	> 150% of normal-appearing tissue	15O-water PET, DSC MRI	Rohi et al. ²²⁰ (also calculated from CBF and CBV values above)
pH	Acidity or alkalinity of tissue (expressed as activity of proton; unitless)	7.2–7.4 (gray and white matter)	<7.0 (tissue)	11C PET, MRS, APT-CEST MRI	Rottenberg et al. ²²¹
CMR _{O2}	Rate of oxygen consumed by tissue (ml O ₂ /100 ml brain/min)	2.8–5.0 ml O ₂ /100 ml brain/min (gray matter) 1.2–1.7 ml O ₂ /100 ml brain/min (white matter)	Largely constant until late stages of ischemia	15O-water PET	Leenders et al. ²¹⁸ Hatazawa et al. ²²²
CMR _{Glc}	Rate of glucose consumed by tissue (ml glucose/100 ml brain/min)	6.1–8.5 ml glucose/100 ml brain/min (gray matter) 2.7–4.1 ml glucose/100 ml brain/min (white matter)	Largely constant until late stages of ischemia Reduction in ischemic core of acute stroke Possible elevation in penumbra regions	15O-water PET (with arterial-jugular venous blood samples)	Scheinberg et al. ²²³ Phepels ²²⁴ Huang et al. ²²⁵ Heiss et al. ²²⁶

Values represent ranges based on literature studies and are approximate. Measurement tools are not exhaustive, but summarize the most popular methods for each category.

CBF: cerebral blood flow; PET: positron emission tomography; CT: computed tomography; DSC: dynamic contrast susceptibility; MRI: magnetic resonance imaging; ASL: arterial spin labeling; CBV: cerebral blood volume; OEF: oxygen extraction fraction; SWI: susceptibility weighted imaging; MTT: mean transit time; MRS: magnetic resonance spectroscopy; APT: Amide proton transfer; CEST: chemical exchange saturation transfer; CMR_{O2}: cerebral metabolic rate of oxygen; CMR_{Glc}: cerebral metabolic rate of glucose.

oxygen delivery as a result of hemoglobinopathies. While the etiology of stroke is well-known compared to most other debilitating neurological conditions, identifying stroke risk factors prior to complete vessel occlusion and the presence or absence of corresponding tissue-level hemodynamic compensation strategies is more complex and an active area of research.

More specifically, in the presence of macrovascular steno-occlusion and corresponding reductions in cerebral perfusion pressure (CPP; difference between mean arterial pressure and venous backpressure), brain parenchyma may adequately compensate for such changes and require minimal or no intervention, or may inadequately compensate and therefore require medical management and/or revascularization therapies. CBF can be maintained at the tissue-level through either collateral flow or autoregulatory increases in cerebral blood volume (CBV; ml blood/100 g tissue). Cerebral autoregulation maintains CPP through vasoconstriction of pial arterioles if mean arterial pressure increases, and through vasodilation if blood pressure decreases, which alters vascular resistance and increases CBV,⁸ although these changes can be small in many patients.⁹ If these compensatory phenomena are inadequate to maintain oxygen delivery, then a progressive decrease in CBF and concomitant increase in oxygen extraction fraction (OEF; ratio of oxygen consumed to oxygen delivered) to maintain CMR_{O_2} ^{10–12} occurs (Figure 1). OEF has been postulated to be a more sensitive indicator of critical tissue-level impairment for cerebral ischemia and eventual strokes, compared to CBF or CBV, over a larger range of hemodynamic impairment^{13,14} and as discussed below, direct OEF measurements using 15O-water positron emission tomography (PET),¹⁵ and more recently indirect OEF measurements using magnetic resonance imaging (MRI), have emerged as relevant tools.

The extent of intracranial vascular stenosis, and the presence or absence of collaterals, measured from angiography, have traditionally been used as surrogates for disease severity and stroke risk. When possible, angiography is complemented with anatomical imaging using computed tomography (CT) or diffusion-, T₂-, and T₁-weighted MRI to gauge acute ischemia, chronic infarcts, and tissue structure and edema, respectively. While these methods are hallmarks of stroke risk determination, they provide no information on how the arterial stenosis translates to parenchymal impairment at the tissue level. As such, more sophisticated diagnostic tools capable of recording additional observables of hemodynamic impairment are necessary to improve our understanding of CVD pathophysiology. The relevance of these measurements depends on stroke etiology and treatment avenues available.

Visualization of sub-clinical disease processes

Modifiable risk factors

The purpose of this document is to summarize the pathophysiology of CVD and the visualization of disease processes (i.e. accumulating pathology) that lead to clinical events and outcomes. However, approximately half of strokes are attributable to causal and modifiable risk factors, as elegantly outlined in a population-based cohort study.³ The impact of a risk factor on stroke burden can be quantified in terms of the population attributable risk,¹⁶ or the proportion of strokes that would not have occurred had the risk factor been absent. Table 2 provides a summary of modifiable risk factors for ischemic and hemorrhagic stroke. It should also be noted that additional risk factors may become discernable with more comprehensive monitoring and screening; for instance, atrial fibrillation has a low population attributable risk, but it has recently been demonstrated with non-invasive 30-day ambulatory monitoring that paroxysmal atrial fibrillation may often go undiagnosed. More comprehensive surveillance of patients extending beyond hospital discharge is likely relevant for effectively managing the spectrum of vascular disease risk factors.¹⁷

Atherosclerotic steno-occlusive disease

Extracranial atherosclerotic disease (ECAD) is a well-known risk factor for stroke. Following the North American Stenting vs. Carotid Endarterectomy Trial (NASCET), patients with symptomatic ECAD of the internal carotid artery (ICA) have been surgically revascularized with carotid endarterectomy, resulting in a 2–4% two-year rate of disabling stroke in patients without perioperative complications and approximately a 17% reduction of stroke compared to similar patients on medical management only.^{18,19} However, patients with intracranial atherosclerotic disease (ICAD) comprise 7–24% of new strokes^{20–23} and appropriate treatment for ICAD is less clear, particularly in the wake of the recently halted Stenting vs. Aggressive Medical Management in Patients at Risk for Stroke with Intracranial Stenosis (SAMMPRIS) and Vitesse Intracranial Stent Study for Acute Ischemic Stroke Therapy (VISSIT) trials, which evaluated the efficacy of new intracranial stents.^{24,25} In these prospective trials, 14–24.1% of patients with ICAD treated with stenting and aggressive medical management (AMM), consisting of anti-platelet and statin therapy, experienced a stroke within 30 days, compared to just 5.8–9.4% of patients receiving AMM alone. Final results from both trials revealed that even in the AMM arms, a high 12.2–15.1% of ICAD patients experienced recurrent stroke in one year.²⁶ There remains a pressing

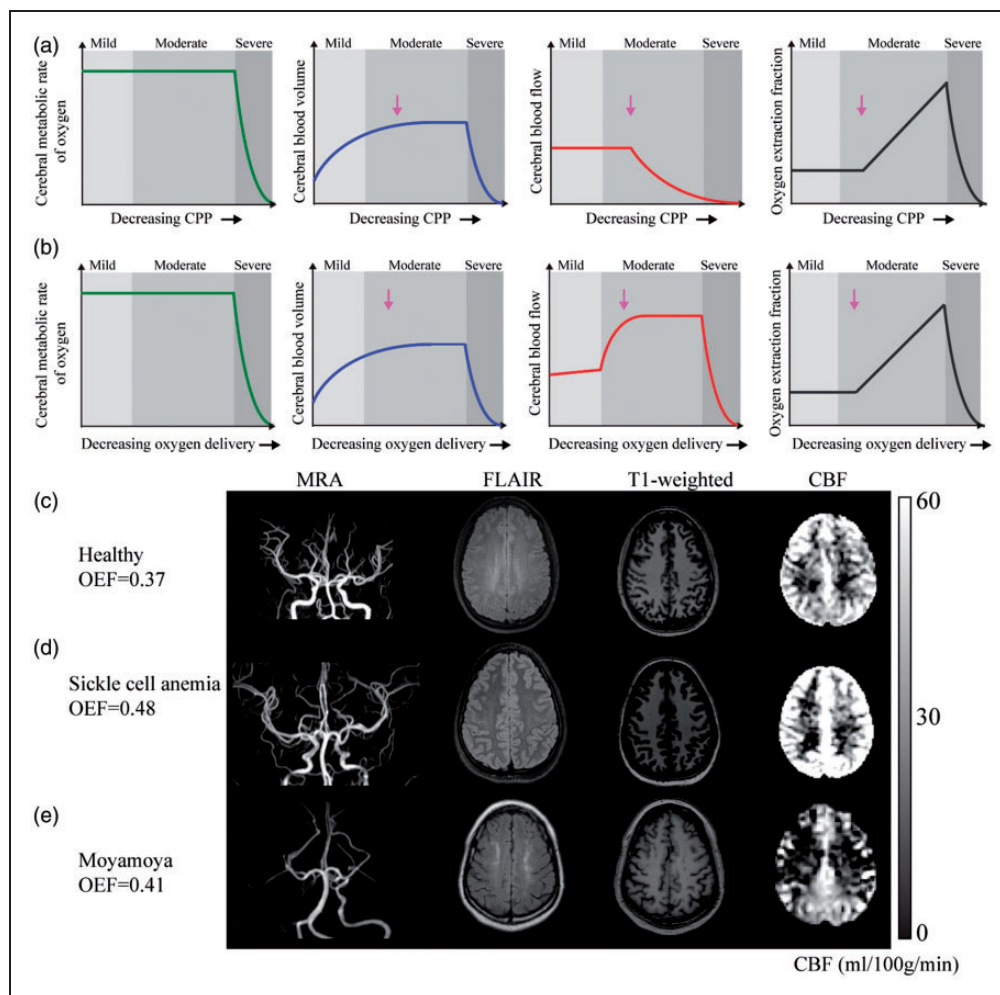


Figure 1. Mechanistic model for increasing stages of hemo-metabolic impairment in (a) ischemia and (b) anemia. In ischemia, as CPP declines the cerebral metabolic rate of oxygen consumption remains constant until CPP is severely reduced. By contrast, CBF at the tissue level may be maintained by collateral flow and/or autoregulation. In moderate disease stages, arteriole cerebral blood volume generally increases via vasodilation to maintain CBF, and CBF begins to increase sharply to maintain adequate delivery of oxygen to tissue. When collateral flow and autoregulation are insufficient to maintain CBF, CBF plateaus or declines and OEF will begin to increase. In anemia, the cerebral metabolic rate of oxygen consumption similarly remains constant until severe impairment. In cases when oxygen can no longer be supplied by these mechanisms, a stroke occurs. Below (c–e) individual cases of structural, CBF, and OEF mapping. (c) A healthy control participant with a normal OEF, and normal findings on anatomical and CBF imaging. (d) A participant with SCA and (e) reduced CPP secondary to bilateral moyamoya disease. The participant with SCA demonstrates elevated CBF in the setting of decreased oxygen carrying capacity of hemoglobin and increased OEF (OEF = 0.48). The participant with bilateral moyamoya with lenticulostriate collaterals, demonstrates right and left anterior and middle cerebral artery territory infarcts seen on FLAIR, bilateral anterior-territory hypoperfusion, and globally elevated OEF (OEF = 0.41) relative to control data. It is possible that ASL MRI, used here, underestimates the true CBF in this patient (see text). Additional details can be found in Watchmaker et al.⁵⁰ and Jordan et al.⁵²

CPP: cerebral perfusion pressure; CBF: cerebral blood flow; OEF: oxygen extraction fraction; SCA: sickle cell anemia; ASL: arterial spin labeling; MRI: magnetic resonance imaging.

clinical need to understand stroke risk factors in these patients.

An analysis of the hazard ratio (HR) of SAMMPRIS patients in the AMM arm presenting with stroke showed that patients with recurrent stroke had a higher incidence of (i) being female (HR = 1.9),

(ii) diabetes mellitus (HR = 1.8), (iii) not taking a statin at enrollment (HR = 2.6), (iv) Rankin grade ≥ 1 (HR = 2.3), (v) old infarct in stenotic artery territory (HR = 2.6), and (vi) stenosis $>80\%$ (HR = 1.9) at mild ($p < 0.10$) significance on bivariate analysis, however only (iii) and (v) met rigorous criteria ($p < 0.05$) on

Table 2. Data from 6844 adults are reproduced from Bos et al.³

Etiological factor for acute ischemic stroke (610/6844)	Population attributable risk, PAR (95% CI)	Etiological factor for hemorrhagic stroke (103/6844)	Population attributable risk, PAR (95% CI)
Hypertension	0.33 (0.20–0.49)	Hypertension	0.24 (0.04–0.73)
Smoking	0.16 (0.08–0.30)	Smoking	0.40 (0.22–0.60)
Diabetes mellitus	0.03 (0.01–0.08)	Diabetes mellitus	0.03 (0.00–0.26)
Atrial fibrillation	0.00 (0.00–0.16)	TC/HDL ratio	0.31 (0.11–0.63)
Coronary disease	0.03 (0.01–0.08)		
Overweight/obesity	0.12 (0.05–0.27)		
TC/HDL ratio	0.03 (0.00–0.82)		
Total	0.55 (0.41–0.68)	Total	0.70 (0.45–0.87)

Data show the PAR for various risk factors with respect to any first-ever ischemic or hemorrhagic stroke. The population attributable risk can be interpreted as the percentage of strokes that can theoretically be prevented if that specific risk factor could effectively and completely be eliminated from the population. These PAR values are calculated taking into account possible confounding and interaction effects across each other. Values are presented with 95% CIs. The numbers presented in this table are slightly lower than those reported earlier in literature^{227,228} since in these data interaction effects and overlap across risk factors are taken into account in the statistical analysis.

PAR: population attributable risk; CI: confidence interval; TC: total cholesterol; HDL: high-density lipoprotein.

multivariable analysis.²⁷ The observed link between a lack of statin regimen at time of stroke and subsequent, recurrent stroke partly motivates the need for vessel wall and plaque stabilization imaging.²⁸ It is thus anticipated that lifestyle, macrovascular, and microvascular changes likely contribute to recurrent stroke risk in patients with ICAD; however, the quantitative relationship between these risk factors and whether short-term changes in these parameters are prognostic for AMM failure remains to be evaluated.

Non-atherosclerotic steno-occlusive disease

Non-atherosclerotic conditions such as moyamoya disease (MMD), characterized by progressive stenosis of the supraclinoid ICA and proximal branches, and the corresponding development of networks of collateral blood vessels,²⁹ places individuals at more than a seven-fold increased risk of stroke.³⁰ While such idiopathic MMD is relatively rare (incidence < 0.9 cases/100,000 children in North America), Moyamoya syndrome (MMS), which may be associated with Down syndrome, sickle cell disease, atherosclerosis, cranial radiotherapy, and a number of other conditions, is observed in the general population and shares many phenotypical characteristics with idiopathic MMD.^{31–34} Such patients have a wide clinical presentation and prognosis, which is hypothesized to depend sensitively on the location and extent of steno-occlusion, parenchymal response via development of collateral vessels, and associated comorbidities.^{29,35} Moyamoya etiology remains unknown, animal disease models do not exist, biomarkers that may place patients at highest risk for stroke have not been conclusively established, and randomized trials evaluating

utility of surgical revascularization have not been performed.

There is currently no treatment that is known to halt or reverse MMS. Treatment focuses on improving CBF through medical therapy with antiplatelet agents, calcium-channel blockers, and more rarely anticoagulants.^{36,37} More aggressive surgical revascularization using either direct bypass or indirect synangiosis procedures are performed in patients with symptoms unresponsive to medical therapy³⁷ and are increasingly utilized, despite the absence of formal proof of efficacy.³⁸ The most pressing clinical question in these patients is whether aggressive surgical procedures are necessary and if so, how tissue-level hemodynamic and metabolic responses may alter stroke risk. Addressing these issues likely requires accurate measurements of how parenchyma compensates for steno-occlusion, including knowledge of (i) vessel lumen and wall morphology, (ii) collateral vessel structure and function, (iii) tissue perfusion and metabolism, and (iv) cerebrovascular reserve capacity.^{39–42}

Sickle cell anemia (SCA) and hemoglobinopathies

SCA is a well-characterized monogenetic disorder with a high prevalence of cerebral vasculopathy, silent cerebral infarct (SCI; infarct on MRI but no focal deficits on neurological exam), and stroke. Hemoglobin S leads to sickled red blood cells, chronic hemolytic anemia, and decreased oxygen carrying capacity. Approximately 40% of children with SCA will have an overt stroke or SCI by age 18 years.^{43,44} Standard care for children with SCA with either overt strokes or SCIs is regular blood transfusion therapy (approximately monthly) for an indefinite period of time for secondary prevention of

cerebral infarct recurrence.^{45,46} The TWITCH trial⁴⁷ recently showed that children with SCA who are receiving monthly blood transfusions for primary stroke prevention can be safely transitioned to oral hydroxyurea after one year. Now a major focus of research in SCA is to identify an optimal strategy for secondary stroke prevention. Despite regular blood transfusion therapy, over a course of five years, 45% of SCA children with overt strokes will have a new infarct recurrence (overt or SCI)⁴⁸ and 9.5% of those with SCI will have a new infarct recurrence (overt or SCI).⁴⁹ The most pressing clinical problem in this high-risk population of children with SCA is to separate the subgroup with pre-existing cerebral infarcts into those (i) likely to progress despite receiving blood transfusion or hydroxyurea therapy and (ii) that either do not require indefinite blood transfusion therapy or require no therapy. Improved imaging techniques are urgently needed to identify children and adults with strokes or SCI that require more aggressive treatment. Imaging methods that assess aspects of cerebral hemodynamics and metabolism such as CBF, CMR_{O₂}, cerebrovascular reserve, and OEF hold promise^{50–52} (Figure 1).

Diagnostic tests for evaluating AIS risk

Patients with neurological symptoms consistent with CVD, including transient ischemic attacks (TIA), generally undergo anatomical imaging and angiography to identify the source of disease and optimal treatment. Multiple modalities including ultrasound, digital subtraction angiography (DSA), CT, and MRI are available as diagnostic tests in patients with suspected CVD.

Ultrasound is primarily used for stenosis grading of the extracranial segments of the ICAs. The advantages of ultrasound include lower cost relative to other imaging methods and lack of ionizing radiation. A primary drawback of ultrasound is the need for an acoustic window, limiting its application in intracranial CVD, as well as significant inter-user variability. Intracranial Doppler, when used without concomitant echography, may lead to erroneous interpretations of the cerebral hemodynamics.

CT and computed tomography angiography (CTA) are widely applied in imaging of the head and neck and of the intracranial and extracranial arteries, respectively. For the assessment of hemorrhage or the detection of chronic infarcts, non-enhanced CT of the head can be performed. Non-enhanced CT scans may evaluate for the presence of arterial calcifications, which are related to future stroke risk in the presence of atheroma.^{53,54} CTA is able to detect steno-occlusive disease of the great vessels, cervical and intracranial vasculature. The advantages of CTA include availability in most hospitals, lack of most contraindications, and the

visualization of the complete trajectory of the vasculature from the aortic arch to the more peripheral intracranial arteries. Limitations are requirements of ionizing radiation and potential side effects of the use of iodinated contrast (allergic reactions, nephrotoxicity).

DSA may be used for both diagnostic and therapeutic purposes. Diagnostic DSA has largely been replaced by CTA, a less-invasive alternative. Currently, DSA is more often used in these patients for therapeutic interventions, such as thrombectomy, and less often for diagnostic purposes only, although some rare causes of recurrent AIS, such as diaphragms of neck arteries may be missed by CTA.⁵⁵ Still, DSA remains the gold standard for assessment of collateral vessels in patients with intracranial steno-occlusive disease and for evaluation of intracranial vascular malformations such as arteriovenous malformations and fistula. Furthermore, it should be noted that the inclusion and stratification of many therapeutic trials (such as the NASCET > 70% stenosis criteria) were based on DSA. The advantages of DSA are its high temporal and spatial resolution. The limitations are that it is an invasive and expensive procedure, ionizing radiation is required, and it carries risks of complications such as stroke or groin hematoma.

Anatomical MRI and magnetic resonance angiography (MRA) are also widely applied in patients with steno-occlusive disease. The role of anatomical MRI is to identify the presence of recent (acute-subacute) and remote infarcts, evaluate the burden of small vessel disease, evaluate for presence of micro- and macrohemorrhage, and exclude alternative etiologies. The location of the cerebral infarcts may help to identify the cause according to the Trial of Org 10172 in Acute Stroke Treatment (TOAST) sub-classifications (cardiac causes, large artery causes, small artery causes, other defined causes, unknown causes),⁵⁶ which have recently been refined to reduce the number of patients with stroke of undetermined cause.^{57–59} Infarcts in multiple perfusion territories may indicate the presence of a cardiac cause of cerebral infarcts, such as emboli in a patient with atrial fibrillation or after cardiac interventions although similar findings might be observed in small vessel diseases.⁶⁰ An infarct in the deep gray or white matter may indicate the presence of small vessel disease (arteriolosclerosis). The burden of small vessel disease can be assessed based on the presence of white matter lesions and remote lacunar infarcts.^{61,62} In recent articles, the standardized assessment of this small vessel disease was explained based on the STandards for ReportIng Vascular changes on nEuroimaging (STRIVE) criteria.⁶³ This included imaging protocols and the proposed terms and imaging features of white matter hyperintensities of presumed vascular origin, lacunes of presumed vascular origin,

recent small infarcts, and perivascular spaces. Furthermore, the presence, location and severity of microbleeds can be assessed with T_2^* or susceptibility weighted imaging (SWI), or quantitative susceptibility mapping (QSM) with either the hypertensive pattern (deep gray matter region) or cerebral amyloid angiopathy pattern (lobar and posterior region).

MRA allows for assessment of the vasculature without the use of ionizing radiation. Contrast-enhanced or phase contrast MRA of the extracranial vasculature allows for diagnosis of arterial stenosis and aids in management decisions, such as whether to perform carotid endarterectomy. Phase contrast MRA may also be used to quantify the blood flow velocity in milliliters per minute. MRA of the intracranial arteries can either be based on contrast enhanced angiography or high-resolution time-of-flight (TOF) acquisition, which may provide a detailed evaluation of intracranial vasculature.

PET imaging may be relevant in more unique cerebrovascular scenarios. Fluorodeoxyglucose 18F (FDG) PET imaging will show the reduction or absence of glucose metabolism in patients with an acute or chronic infarct. PET imaging with 15O-tracers can directly measure CBF, CBV, and OEF. PET/MRI has also been shown to be feasible in the early stroke period.⁶⁴ 15O-water PET may show the presence of an increased OEF in patients with chronic arterial occlusion and 15O-water PET has been studied for the selection of patients for extracranial–intracranial bypass surgery in patients with carotid occlusion.⁶⁵ Based on functional PET imaging, a classification of brain tissue and patients with different severity of hemodynamic impairment has been proposed, with stage-1 indicating an autoregulatory increase in CBV and stage-2 an increase in OEF. The Carotid Occlusion Surgery Study (COSS) trial⁶⁵ evaluated the efficacy of intracranial-extracranial bypass surgery in patients with a carotid occlusion with hemodynamic cerebral ischemia identified by ipsilateral increased OEF, as measured by PET. The COSS study showed no difference in outcome (stroke recurrence) between the operated and the non-operated group, although later re-analysis questioned whether the OEF methodology used was adequate.⁶⁶ The COSS study highlights the challenges of PET imaging, including invasive blood sampling, radiation dose, complex procedures, and need for a cyclotron to produce short-lived tracers and motivates development of noninvasive imaging methods to measure tissue physiology. In clinical CVD research, novel PET tracers such as those targeting microglia and macrophages have emerged to assess the regional and global cerebral inflammatory reaction after brain infarcts. An example in clinical research is the use of specific PET tracers to assess the regional and global cerebral inflammatory reaction after brain infarcts.⁶⁷

Figure 2 highlights the role of multi-modal imaging in the diagnosis of patients with distinct CVD.

Emerging MR neuroimaging methods

New developments in MRI enable better depiction of all sub-parts of the vascular tree, including the large vasculature, the structure and flow through the microvascular bed, as well as characterization of the intracranial vessel wall.

Recently developed MRI techniques include intracranial vessel wall imaging, which may help to differentiate causes of intracranial stenosis such as arterial vasculitis, reversible vasoconstriction syndrome (RVCS), moyamoya, and atherosclerosis (Figure 2). Intracranial arterial vasculitis will result in enhancement of the vessel walls of intracranial arteries. RVCS will demonstrate arterial stenosis without vessel wall enhancement.⁶⁸ Moyamoya will result in circumferential narrowing of the supraclinoid ICAs with collateral formation. Intracranial atherosclerosis may result in enhancing intracranial arterial vessel wall lesions that are most often eccentrically located with typical locations such as the distal ICA just before the bifurcation, the middle cerebral artery (MCA), and the distal vertebral artery.

There has been a recent increase in the use of functional measures of the cerebrovasculature, especially with MRI. One parameter of interest is cerebrovascular reactivity (CVR), defined broadly as the ability of vessels to increase CBV in response to a vasoactive stimulus. Here, either mild hypercapnia (3–6% CO_2 administration), breath-holds, or acetazolamide are utilized to alter blood CO_2 content, which leads to vasodilation and a concomitant increase in CBF and CBV in compliant vasculature. During this challenge paradigm, quantitative CBF measurements (CT, MRI, or PET) or more recently blood oxygenation level-dependent (BOLD) MRI measurements (Figures 3 and 4) can be used. For instance, for respiratory hypercapnic stimuli, a 0.2–0.4% BOLD increase per mmHg increase in end-tidal CO_2 at 3 T is typical for healthy tissue. The BOLD signal provides an indirect marker of this change in CBF and CBV and can be used to assess the reserve and thereby the health status of the smaller intracranial vasculature, not currently visualized with angiography. In pathological conditions, CPP decreases and arterioles at the tissue-level will dilate to increase CBF through autoregulation. When this relaxation becomes maximal, the autoregulatory capacity is exhausted, and any additional vasodilatory challenge leads to a shunted or negligible CBF and CBV increase.

Arterial spin labeling (ASL) CBF-weighted MRI can be used to quantify CBF changes during a physiological challenge more directly. Unlike CBF methods that require injection of an exogenous contrast agent, in

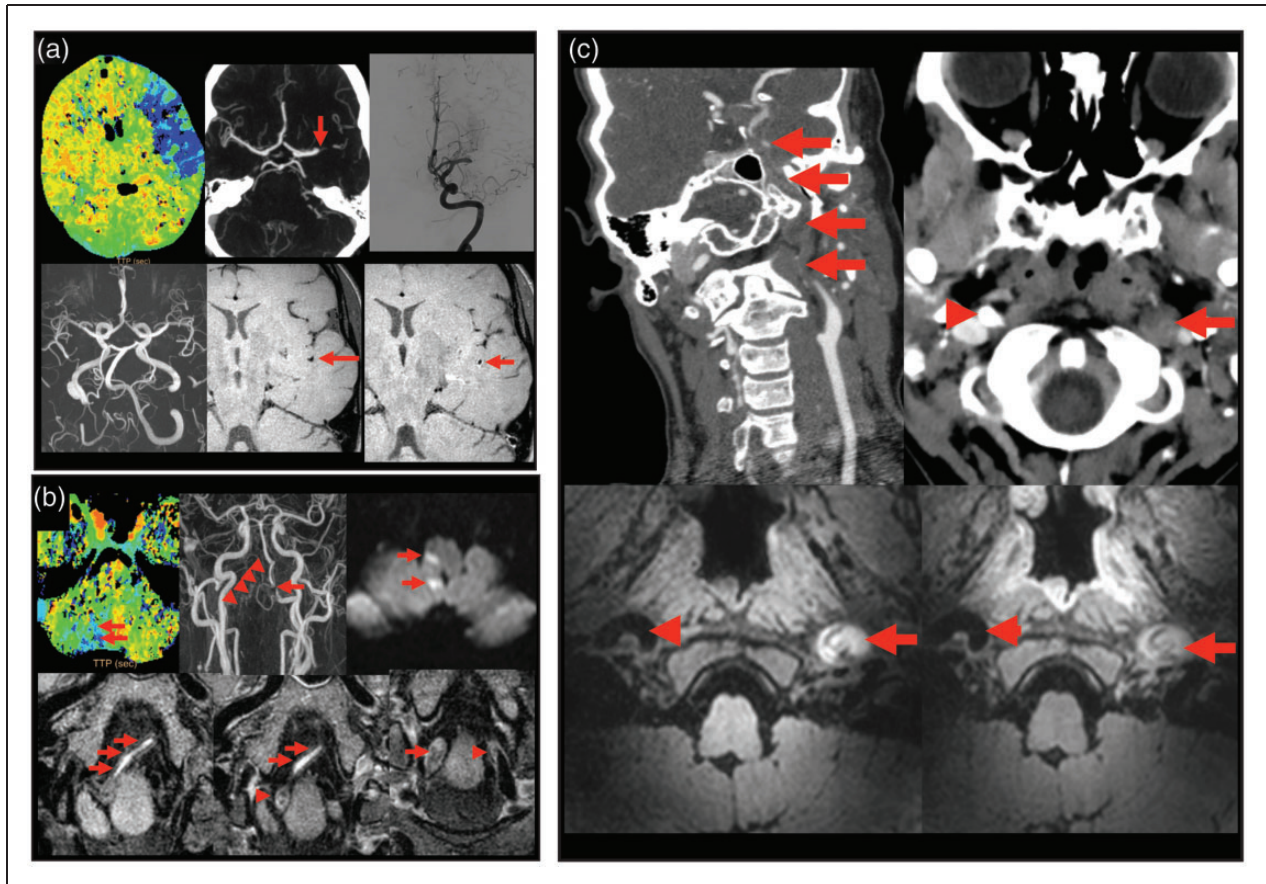


Figure 2. Relevance of multi-modal imaging for diagnosing CVD. (a) Top row left-to-right: CT perfusion (time to peak) shows delayed arrival (blue) in a large area of the left middle cerebral artery perfusion territory. CTA shows an acute stop in the M1 segment of the left middle cerebral artery occlusion (red arrow). Angiography prior to the thrombectomy procedure confirmed the occlusion of the left M1 segment of the middle cerebral artery. Bottom row left-to-right: TOF MR angiography after the thrombectomy showed complete revascularization of the left middle cerebral artery. The high resolution black blood vessel wall MRI sequences before (middle) and after contrast (right) shows faint vessel wall enhancement of the wall of an M2 segment on the side with the recanalized middle cerebral artery. (b) Top row left-to-right: CTP (time to peak) shows delayed arrival in a small area of the right cerebellum (arrows). Contrast-enhanced MR angiography shows no contrast filling of the right distal vertebral artery (arrow heads) and a focal stenosis of the distal left vertebral artery (arrow). Diffusion-weighted imaging shows small focal ischemic regions of the medulla oblongata and right cerebellum (arrows). Bottom row left-to-right: the high resolution black blood vessel wall MRI sequences before (left) and after contrast (middle) shows both before and after contrast a T1 hyperintense occlusive thrombus (arrows) in the center of the right distal vertebral artery. In the more proximal intracranial vertebral artery (image on the right), an atherosclerotic plaque can be seen which is less hyperintense on this vessel wall MRI sequence compared to the thrombus. An occlusive atherosclerotic plaque is present on the right side (arrow) and a non-occlusive plaque is present on the left side (arrowhead). (c) Dissection of the left internal carotid artery. Top row left-to-right: coronal reconstruction of a CTA shows occlusion of the left internal carotid artery (arrows). The occlusion starts a few centimeters after the carotid bifurcation with a tapering of the lumen of the left internal carotid artery. The lumen of the distal intracranial internal carotid artery shows contrast opacification. Axial CT angiographic images show enlargement of the left internal carotid artery just below the skull base (arrow) with no contrast opacification. The right internal carotid artery shows high density signal (arrowhead) due to the contrast opacification. Bottom row left-to-right: the high resolution black blood vessel wall MRI sequences before (left) and after contrast (right) shows both before and after contrast a T1 hyperintense signal due to the mural thrombus with no clear contrast enhancement.

CVD: cerebrovascular disease; CTA: computed tomography angiography; TOF: time of flight; MR: magnetic resonance; CTP: computed tomography perfusion.

ASL endogenous blood water is magnetically labeled non-invasively using a single radiofrequency pulse or a combination of radiofrequency pulses. The SNR of ASL-MRI is much lower than that of BOLD MRI.

However, the contrast-to-noise ratio (CNR), for instance in response to vasoactive stimuli, is similar for BOLD and ASL, as the T_2^* change that underlies the BOLD effect is small ($< 10\%$ at 1.5 T–3.0 T) but the

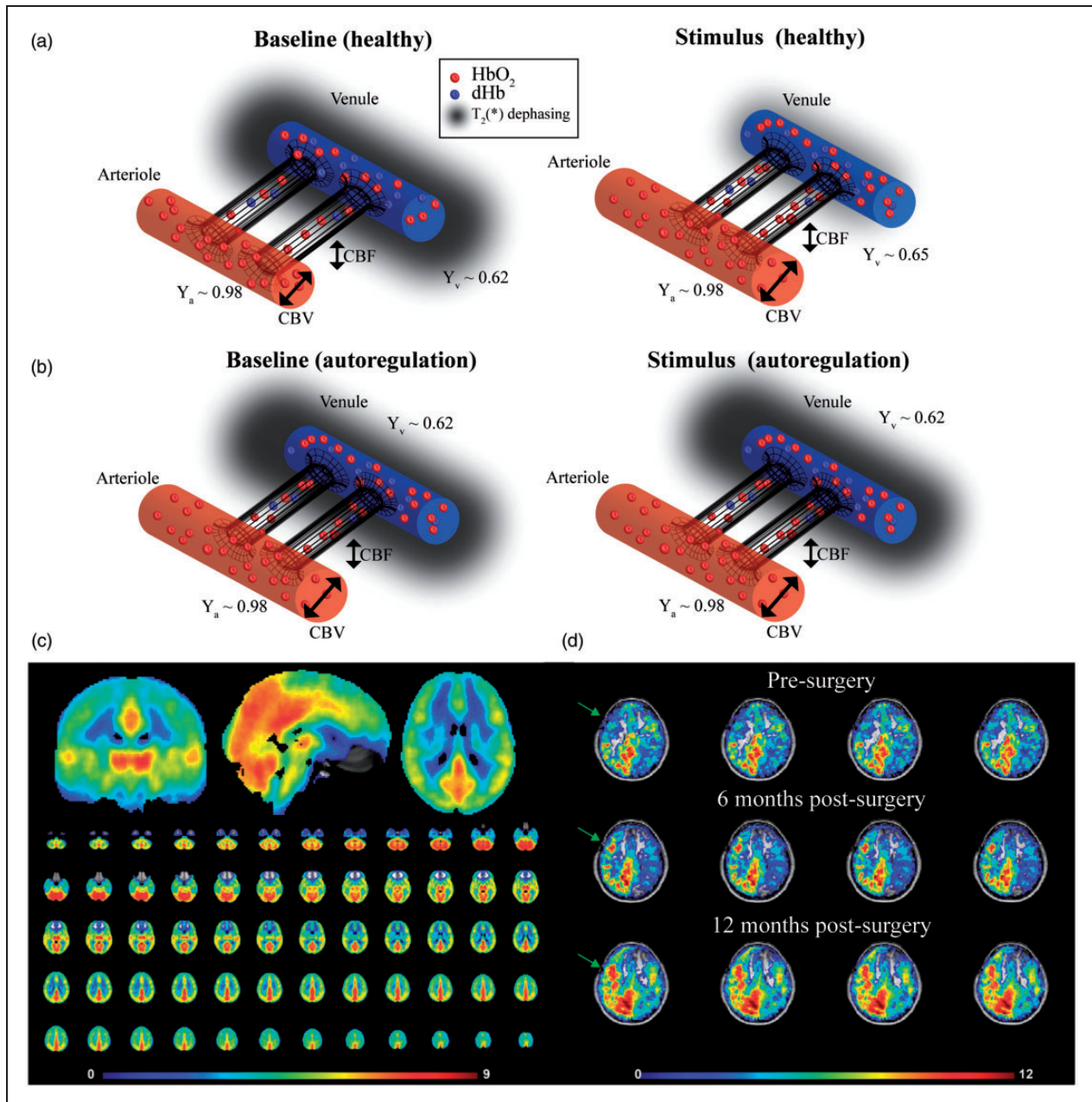


Figure 3. Physiology of CVR-weighted imaging with BOLD MRI. (a) Relaxation of smooth muscle lining arterioles elicits increases in blood flow; for largely isometabolic stimuli such as hypercapnia, this translates to a decrease in paramagnetic dHb concentration in venules and an increase in BOLD signal. The gray shadow surrounding the venules indicates local field (and signal) dephasing from dHb. (b) In pathological conditions with high CPP, smooth muscle relaxation is reduced due to elevated CBV at baseline (i.e. elevated autoregulatory capacity), hyperemia is shunted or negligible, leading to minimal change in venous dHb and a small or negligible BOLD response. (c) Mean CVR-weighted maps from BOLD MRI in healthy volunteers (mean over $n = 50$) yield largely symmetric CVR; orthogonal representations shown above along with individual axial slices. (d) A patient with bilateral moyamoya disease scanned before and at two time points after right-sided surgical revascularization with EDAS. CVR-weighted increases are seen focally at six months, and larger CVR-weighted increases consistent with more extensive angiogenesis are visible at the second follow-up. CVR: cerebrovascular reactivity; BOLD: blood oxygenation level dependent; MRI: magnetic resonance imaging; dHb: deoxy-hemoglobin; CPP: cerebral perfusion pressure; EDAS: encephaloduroarteriosynangiosis; Y_a : arterial oxygen saturation; Y_v : venous oxygen saturation; CBF: cerebral blood flow; CBV: cerebral blood volume. Additional information can be found in Donahue et al.^{215,216}

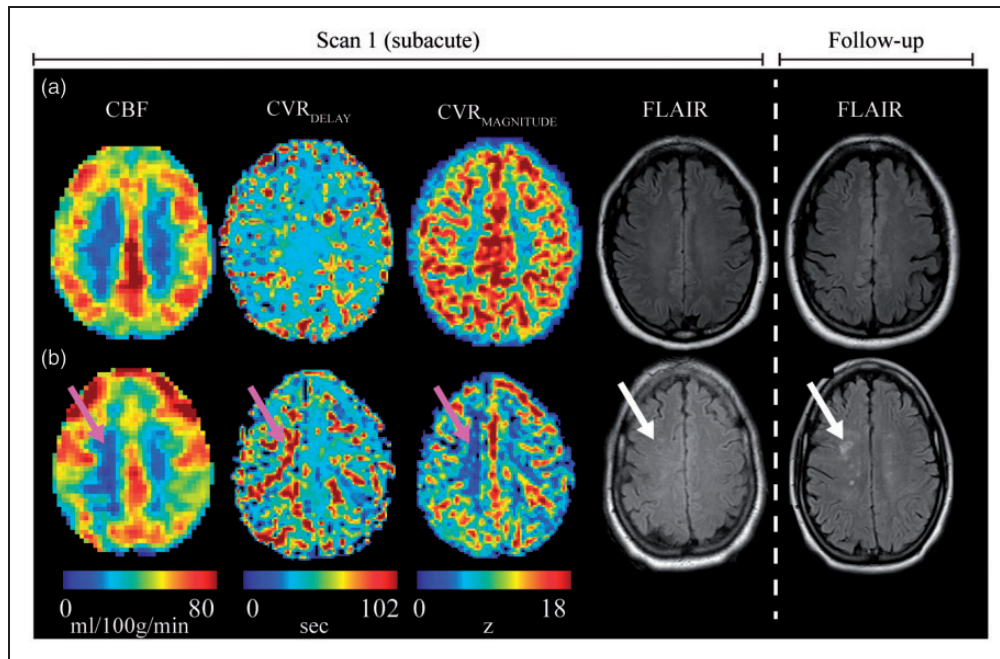


Figure 4. Potential of personalized stroke risk assessment using hemodynamic measurements of CBF from non-invasive arterial spin labeling MRI, time for parenchyma to increase CBF and CBV in response to mildly hypercapnic respiratory stimulus (CVR_{DELAY}), and the maximum CVR ($CVR_{MAGNITUDE}$) obtained from hypercapnic BOLD MRI. Data are shown for two patients scanned within 45 days of AIS (left). (a) Fifty-two-year female with bilateral M2 stenoses and significant left P2 stenosis. CBF, CVR_{DELAY} and $CVR_{MAGNITUDE}$ are symmetric; 1.3-year follow-up shows no new infarcts. (b) Forty-nine-year female with stenosis of the intracranial right internal carotid artery. CBF and reactivity appear reduced, and CVR_{DELAY} increased, in identical regions, yet there is no infarct present at presentation. At 108 days, new foci of acute infarct within the right centrum semiovale in a watershed distribution are observed (white arrow). The images highlight the possibility of using impaired hemodynamic patterns to predict recurrent stroke, however additional trials in more subjects are required.

CBF: cerebral blood flow; MRI: magnetic resonance imaging; CBV: cerebral blood volume; CVR: cerebrovascular reactivity; BOLD; blood oxygenation level dependent; AIS: acute ischemic stroke.

CBF change is much larger (20–50% for analogous stimuli).⁶⁹ Whereas BOLD provides an indirect measure of CBF and CBV changes through capillary, tissue, and venous water relaxation time changes, ASL provides a more direct measure of CBF.

Technical advancements are also improving the quality of these and related methods. By advanced k -space sharing techniques and compressed sensing, the acquisition of 4D contrast-enhanced MRA data can be performed at ever-higher spatial and temporal resolution.^{70–72} Cerebrovascular applications of compressed sensing have been limited. However, recent developments in non-contrast enhanced MRA based upon ASL-like sequences have emerged as an attractive alternative enabling high quality 4D MRA within reasonable scan-times. New developments include improved readout strategies, such as golden angle radial reconstructions, which enable postponement of any decision on the trade-off between spatial and temporal resolution from the acquisition to the reconstruction phase of the sequence, thereby offering higher flexibility. Additionally, ASL-MRA has the

advantage that it enables the possibility to restrict the labeling to a single artery, thereby allowing selective depiction of the vascular tree.^{73–75} Recent ASL advancements also allow for the vascular source of the blood to be identified, using vessel-selective ASL,^{76–78} which should have relevance for visualizing collateralization (Figure 5).

Non-invasive CBF imaging by ASL has been mostly accepted for clinical applications,⁷⁹ and includes a consensus statement by the perfusion study group of the International Society for Magnetic Resonance in Medicine (ISMRM) and the European Cooperation in Science and Technology (EU-COST) Action.⁷⁹ However, applications of ASL in CVDs are challenging in the presence of unknown and long blood transit times. CBF underestimation may occur if labeled blood water may not yet have reached the imaging slab when the readout commences, and focal overestimation may occur if the tagged spins remain in large vessels and have not yet perfused into the tissue. Velocity-selective or acceleration-selective ASL provides theoretically more accurate, non-invasive CBF

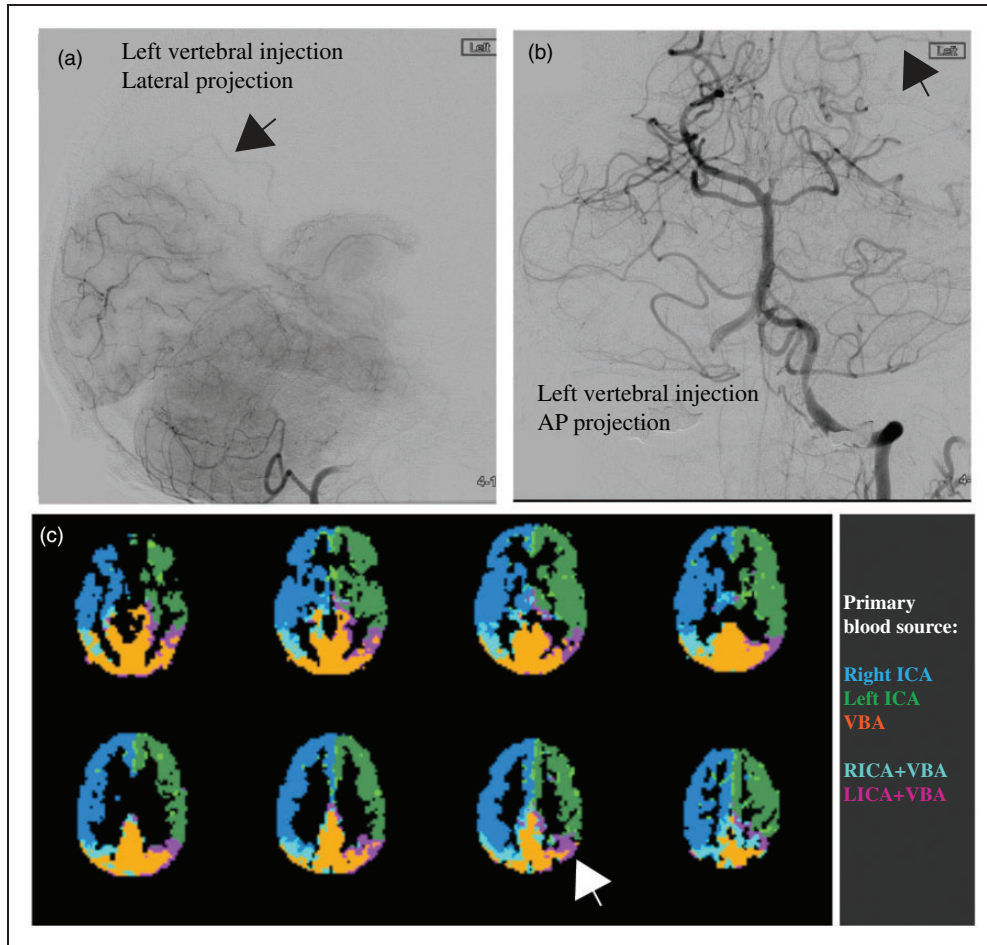


Figure 5. Example of flow territory and collateralization mapping using noninvasive vessel-selective ASL. Left vertebral injection (lateral (a) and AP (b) projections) show filling of left M3 and M6 ASPECTS regions (black arrows). (c) Non-invasive vessel selective ASL with magnetic blood water labeling of left ICA, right ICA, and basilar artery. A fuzzy k-means clustering algorithm was used to cluster the source of the blood flow for each voxel from the different vessels. Mixing is seen between left PCA and MCA territories (white arrow), consistent with angiography. For additional information, see Arteaga et al.²¹⁷

ASL: arterial spin labeling; AP: anteroposterior; ICA: internal carotid artery; PCA: posterior cerebral artery; MCA: middle cerebral artery.

imaging in slow flow conditions,^{80–83} but clinical validation and technical developments are needed to secure widespread clinical acceptance.⁸⁴ Alternatively, one can measure the arterial transit time (ATT) as a hemodynamic parameter of interest in itself, mirroring experiences with dynamic contrast susceptibility perfusion MRI (DSC-MRI) that showed timing parameters to be among the most used perfusion parameters in stroke.⁸⁵ While measurement of ATT with multiple ASL post-label delays^{86,87} comes at a cost of longer scan times, newer strategies allow ATT measurements to be performed in a highly time-efficient manner by using time-encoded ASL.^{88,89}

Furthermore, one can foresee a move toward multi-parametric imaging in CVD. One such approach is to obtain a measure for capillary transit time heterogeneity

from DSC-MRI.^{90,91} By using a combined gradient and spin echo readout during DSC-MRI, complementary information on the microvascular architecture can be obtained.^{92,93} Similarly, CBF MRI can be used to obtain more multi-dimensional microvascular information, for example with MR fingerprinting ASL,⁹⁴ vascular fingerprinting,⁹⁵ introducing flow crushers to probe the microvascular architecture and extracting multi-dimensional microvascular information.⁹⁶

Finally, in recent years, a clear improvement in the depiction of the intracranial vessel wall can be observed, for example by using ultra-high field MRI⁹⁷ and careful sequence design. The interested reader is referred to the recent consensus statement by the Vessel Wall Imaging Study Group of the American Society of Neuroradiology.²⁸

Acute ischemic and hemorrhagic stroke

Prevalence and overview

Acute stroke can be classified into ischemic and hemorrhagic types. Hemorrhagic stroke occurs when rupture of a cerebral artery or vein results in intracranial hemorrhage, and subarachnoid hemorrhage (SAH) and intracerebral hemorrhage (ICH) are the most common causes of hemorrhagic stroke. Non-traumatic SAH affects 30,000 patients per year in the United States (3% of all strokes) and is most commonly caused by rupture of a cerebral artery aneurysm.⁹⁸ Ruptured cerebral aneurysms may be treated by microsurgical clipping or endovascular coil embolization, and brain imaging is essential to guiding treatment.⁹⁸ Patients with SAH are evaluated by CT given the wide availability and rapidity of this technique; the goals of imaging include identifying the presence and distribution of SAH and the presence of hydrocephalus, which may require emergency and life-saving external ventricular drain placement.⁹⁸ Identification and characterization of the ruptured aneurysm is performed by CTA or DSA, and the morphologic appearance of the aneurysm in association with the clinical status of the patient are used to determine whether the patient should undergo surgical or endovascular aneurysm treatment.⁹⁸ There has been a notable trend over the past decade toward endovascular treatment of ruptured cerebral aneurysms. Given the lower invasiveness of this technique,⁹⁹ it is likely that endovascular aneurysm treatment will continue to increase in numbers in the future.

ICH most commonly results from rupture of a perforating artery in patients with long-standing hypertension, and 63,000 patients per year in the United States (7% of all strokes) suffer from ICH.^{100,101} Medical therapy remains the mainstay of treatment of ICH, although surgical hematoma evacuation or hemicraniectomy may be performed to decompress large hematomas.¹⁰¹ CT remains the most commonly used modality for brain imaging in patients with ICH as this modality allows for a rapid and accurate diagnosis. CTA is increasingly used to identify the *spot sign* (i.e. tiny enhancing foci), an imaging biomarker of ICH growth and a poorer prognosis.^{102,103} It will be of interest to determine whether the identification of the spot sign may lead to more aggressive surgical treatment and improved patient outcomes in future studies. Other neuroimaging modalities, such as DSA, have a more limited role in the evaluation of ICH unless there is concern for an underlying tumor or vascular malformation as a cause of the hemorrhage. ASL-MRI has been shown to be quite sensitive to identify arteriovenous malformations (AVM) and dural arteriovenous fistulas (dAVF) in the setting of ICH of unknown cause.^{104–106}

AIS commonly results from thrombotic or thromboembolic cerebral artery occlusion, and approximately 795,000 patients per year in the United States suffer an AIS.¹⁰⁷ AIS related to acute occlusion of large arteries may be treated by intravenous thrombolysis and/or endovascular mechanical thrombectomy (EVT). Antiplatelet agents remain largely prescribed in patients treated later than 4.5 h post-symptom onset, particularly in the absence of arterial occlusion. Since the 1995 National Institute of Neurological Disorders and Stroke trial,¹⁰⁸ brain imaging by CT, and more recently by MRI, has become established as an essential tool to guide treatment of AIS. The goals of brain imaging include identifying the size and extent of cerebral infarction, identifying stroke mimics, and identifying contraindications to treatment such as intracranial hemorrhage.¹⁰⁹ More recently, the role of brain imaging in AIS has been expanded to include vascular imaging for the selection of patients for EVT.^{110–114}

Additionally, advanced brain imaging techniques such as collateral vessel imaging and perfusion imaging to identify the tissue at risk of infarction, or *ischemic penumbra* imaging may play an increasing role in the selection of patients for EVT.^{109,112,113} The ischemic penumbra represents ischemic tissue that may remain viable but is at risk of continuing to infarction unless CBF can be restored by recanalization therapy (Figure 6). Intravenous or intra-arterial administration of recombinant tissue plasminogen activator (tPA) and EVT have been shown to increase reperfusion rates and to reduce final infarct size when administered within the first 4.5 h of symptom onset^{115–117} and additional data has recently been provided that EVT can be effective up to 12-h post-stroke.¹¹⁴ Importantly, recanalization therapy carries the risk of hemorrhagic events, which occur in approximately 6% of patients treated with EVT or tPA.¹¹⁸ Therefore, fast imaging tools are needed that identify patients most likely to benefit from revascularization, and thereby avoid risks of tPA or EVT in futile cases.

Prior to treatment, the infarct core and penumbra are commonly estimated by computed tomography perfusion (CTP) or perfusion- and diffusion-weighted MRI (PWI and DWI). Hyperintense regions on DWI (or hypointense on apparent diffusion coefficient (ADC) maps) are typically thought to represent the ischemic core, yet in some patients, subregions of the DWI lesion may not progress to infarction.^{119,120} Hypoperfused regions on DSC-PWI maps typically include core, penumbra, and areas of benign oligemia in which the tissue survives spontaneously without the need of recanalization^{121–124} and it may be challenging to distinguish these regions in many patients using existing imaging procedures. It is therefore desirable to improve existing and pursue new imaging

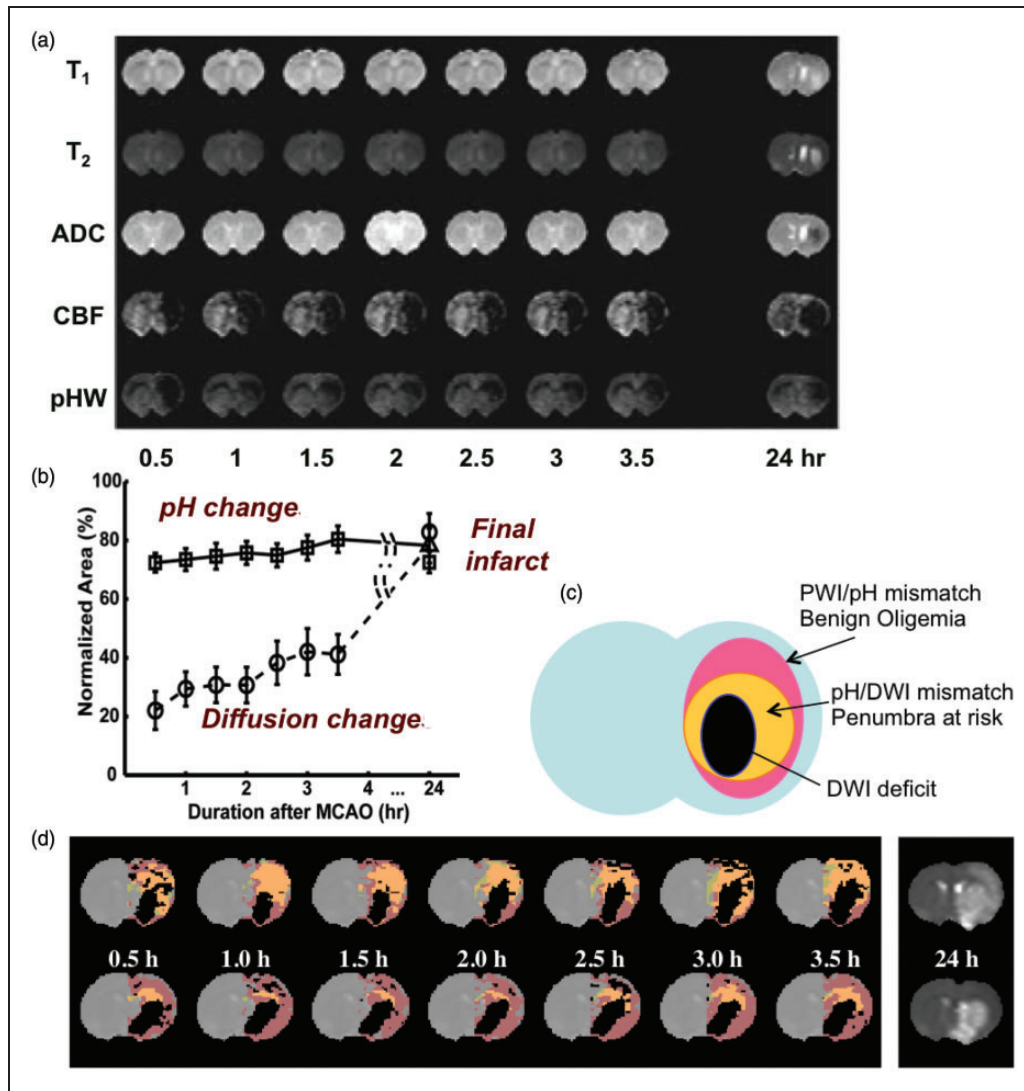


Figure 6. Multi-parameter MRI as a function of time after permanent MCAO in rat. (a) Images of rat in which no T₁, T₂, and ADC changes were seen, but ischemia was confirmed by hemispheric CBF reduction (obtained using arterial spin labeling) as well as a pH-weighted deficit. Hyperintensity in the T₂-weighted image at 24 h gives the final infarction area. (b) Group analysis of ischemic volume evolution for 18 rats with perfusion/diffusion mismatch, comparing areas of pH change and diffusion change as fraction of the perfusion deficit region. The pHw region predicted well the evolution to infarction. (c) Parcellation of ischemic area in terms of three zones, a DWI deficit most likely proceeding to infarction, a pH/DWI mismatch region at risk of infarction and a PWI/pH mismatch not at risk. (d) Processed images for two other animals showing evolution of pHw-deficit (orange) and diffusion deficit (black) with respect to perfusion deficit (purple) as a function of time post-MCAO occlusion. The T₂-weighted image at 24 h shows final infarction area predicted well by diffusion + pHw regions. Reproduced in part, with permission, from Sun et al.¹⁵⁵ MCAO: middle carotid artery occlusion; ADC: apparent diffusion constant; CBF: cerebral blood flow; DWI: diffusion-weighted imaging; PWI: perfusion-weighted imaging.

approaches that may be capable of defining the penumbra more precisely.¹²⁵ It will be of interest to determine whether emerging techniques for penumbra assessment, such as intravoxel incoherent motion, resting-state functional MRI, OEF mapping, or pH mapping have a role in AIS imaging.^{126–128}

Evaluation and management of AIS in the future could be based on evidence gleaned from recent clinical trials that have confirmed the important role of

collateral circulation and related imaging markers. Although the definition of collaterals has historically been limited to the extent of arterial anastomoses providing compensatory blood flow to the ischemic territory at risk, collateral equivalents or imaging markers are now recognized in acute ischemia. For instance, non-contrast CT patterns of hypodensity such as regional Alberta Stroke Programme Early CT Score (ASPECTS)¹²⁹ topography may indirectly

reflect the extent of collateral blood flow in proximal arterial occlusion of the anterior cerebral circulation. After the recent establishment of EVT as a proven strategy to improve the outcome of patients with AIS involving large vessel occlusions (which is still only about 25% of the acute stroke populations), the debate has revolved around how to best select patients for treatment in an unbiased manner (i.e. not on treating patients who would do well regardless of intervention). Future research needs to define the best way to select stroke patients for EVT, without excluding patients who might still benefit. Imaging tools will need to be optimized accordingly.¹³⁰ Most recently, it has been demonstrated that although the prognosis of patients with more extensive baseline lesions on either CT or MRI may be relatively worse, such patients may still benefit from intervention.¹³¹ Recently, enrollment to the DWI or CTP Assessment with Clinical Mismatch in the Triage of Wake-Up and Late Presenting Strokes Undergoing Neurointervention (DAWN) trial was halted due to overwhelming efficacy of mechanical embolectomy with medical therapy vs. medical therapy alone in patients treated 6–24h post-stroke. Information on collateral circulation could be used as a gauge for expectations and in the future to tailor the extent or duration of reperfusion efforts. Even after reperfusion, the serial imaging of infarct patterns and compensatory collateral circulation could be used to manage patients in the acute and subacute phase, but this is an area of future investigation.

Diagnostic tests

Non-contrast CT of the brain for detection of cerebral infarcts has been used for more than three decades and remains a first line imaging method in the setting of acute stroke with the primary role to evaluate for the presence of hemorrhage, a contraindication to intravenous tPA.

CTA has become part of the standard work-up of patients with suspected cerebral infarcts. With thrombectomy as a therapeutic option, the addition of CTA is now required for every stroke center to evaluate for the presence of an occluded intracranial artery that would be amenable to such intervention. In particular, the detection of proximal ICA stenosis will allow for evaluation of endarterectomy in addition to thrombectomy. A possible next step in the application of CTA in the work-up of patients with AIS is the inclusion of the heart in the field-of-view to rule out a cardiac cause of stroke such as thrombi from the heart. Furthermore, the more recently developed technique of multiphase CTA may be applied in the setting of arterial occlusion to detect the presence and extent of collateral vessels.

In the setting of hemorrhagic stroke, CTA may detect potential causes such as a vascular malformation or aneurysm with a predominant parenchymal hemorrhage. The spot sign on CTA may be indicative of acute leakage of contrast from the arterial vasculature, which has been found to be related to a growth of the hemorrhage and a worse prognosis. Finally, CTA may suggest an alternative diagnosis such as venous sinus thrombosis, (peripheral) vasoconstriction, AVM, or arterial-venous fistula.

CTP in AIS imaging has been popular in a clinical research setting in the last decade and is now widely applied in clinical practice. CTP allows for the calculation of CBF, CBV, time to peak (TTP), and mean transit time (MTT; mean time red blood cells spend to traverse the capillary circulation). MTT is also equivalent to the ratio, and identification of areas of ischemia/penumbra (prolonged MTT due to increased CBV and/or decreased CBF) and infarcted tissue (prolonged MTT due to very low CBF) are frequently considered. If there is reperfusion, hyperemia can lead to shortened MTT as well in parenchyma that may or may not be abnormal on DWI. By identifying a region of abnormal perfusion, CTP may aid in detection of peripheral intracranial arterial occlusion. Of note, the additional diagnostic information of CTP on top of patient symptoms and CT/CTA information has been questioned.¹³² Small cerebral areas of ischemia with cellular depolarization (i.e. mostly destined to infarction) may be missed that are readily visible on MRI with DWI.

A typical MRI protocol in acute stroke patients will consist of the following sequences: DWI, T₂-FLAIR, T₂*, and possibly TOF-MRA and DSC-PWI. A primary advantage of MRI is the high sensitivity for small ischemic lesions with DWI sequences. Ruling out hemorrhage with T₂*-weighted sequences is crucial to allow treatment with intravenous tPA, as this sequence has been shown to be equal to or better than CT for this purpose.¹³³ Fast TOF-MRA allows for the identification of the site of intracranial arterial occlusion. However, the quality and resolution of the fast TOF-MRA images may be limited and occlusions of smaller, more peripheral, intracranial arteries may be missed. An alternative method, contrast-enhanced MRA has the advantage that with the imaging during the first passage of the contrast bolus, both the extracranial and intracranial arteries can be imaged with higher CNR. DSC-PWI in acute stroke patients may enhance the detection of the location and extent of an area of ischemia and may be used to evaluate for potential perfusion–diffusion mismatches indicative of infarct growth. MTT is also a relevant indicator of the cerebral circulation as discussed above, and can be assessed from DSC-MRI. In recent years, ASL MRI has also been used for perfusion measurements in acute stroke

patients.^{83,134,135} The limitations of MRI in acute stroke patients in many centers are the restricted availability, higher cost, and imaging time, and not all patients are MR-compatible and screening procedures may add time.

Emerging methods in acute stroke imaging

Expanding the acute stroke imaging infrastructure is inherently difficult, primarily due to time sensitivity, precluding potentially beneficial but time-consuming investigations such as those based on PET, and a general difficulty evaluating novel imaging approaches, which could delay treatment. Beyond these difficulties, major interests remain in the ability to estimate the time of onset in those with unwitnessed strokes, and to portend treatment efficacy, either tPA or EVT, on an individualized basis.

The estimation of stroke onset time may be possible using CT-based water quantification techniques¹³⁶ or MRI-based relaxometry,¹³⁷ enabling treatment to be administered in patients who cannot currently receive it. Triaging patients for treatment beyond currently accepted therapeutic windows would require improved delineation of infarcted tissue (tissue not salvageable), penumbra (tissue at risk but salvageable), and benign oligemia (hypoperfused tissue not at risk). Patients with large penumbra regions may benefit from tPA even after the standard thrombolysis treatment window, but establishing this requires additional clinical trials that likely incorporate neuroimaging. These methods could focus on measuring the extent of collateralization through analyzing DSC source data,^{138,139} the use of vessel-selective ASL techniques, measuring the extent of collateralization through vessel-encoded angiography or perfusion imaging, or measuring OEF, MTT, CMR_{O_2} , and/or pH throughout the ischemic core and penumbra. MR-based methods have been under development for this purpose since the early 1990s.^{140,141} Emerging MRI methods for evaluating OEF and CMR_{O_2} using quantitative BOLD from asymmetric spin echo (ASE)¹⁴² scans, quantitative blood T_2 measurements^{143–146} (which can then be converted to blood oxygenation level), and T_2^* -weighted imaging during hyperoxia¹⁴⁷ hold promise but have not been applied in large-scale human studies. Amide proton transfer (APT) chemical exchange saturation transfer (CEST) MRI utilizes a contrast mechanism that depends on water and amide proton exchange. This exchange rate is base-catalyzed over a physiological range and therefore provides pH sensitivity^{148,149} and may detect ischemic tissue acidosis in the infarct^{150–152} (Figure 6). It is likely that a fast, multimodal protocol which encompasses measurements of diffusion, perfusion, OEF, MTT, oxygen

metabolism, and pH could improve abilities to quantify the spatial extent of the ischemic penumbra, with high apparent ADC indicating tissue likely destined for infarction, but preserved ADC with reduced perfusion,¹⁵³ elevated OEF,¹⁵⁴ and/or moderately reduced pH^{155–157} indicating tissue at risk of infarction but potentially salvageable. Also high and low ADC may indicate infarction, but high ADC can be observed on conventional T_2 -weighted FLAIR, whereas low ADC is suggestive of cytotoxic edema, and often considered infarct core. Testing such hypotheses will require faster scan times for these methods, perhaps facilitated by recent advances in accelerated imaging.^{71,158,159}

Additionally, recent studies have suggested the relevance of collateral evaluation in triaging patients for stroke treatments. Ongoing endovascular trials and registries will provide important data on how collaterals influence the course of late-presenting patients, even beyond the traditional time windows for acute AIS therapies. It remains unknown whether all such patients have more robust collaterals that have sustained them longer or if the same range of collateral grades and perfusion patterns may be seen at these later time points. As future trials are developed to study novel devices and expanded treatment windows, impact of adjunctive medications, anesthesia and other factors, and collateral status will be a required component of such analyses. Emerging data on large-scale registries in acute stroke will also provide important insight on how collaterals vary around the world and impact in a broad range of acute AIS scenarios.

Stroke recovery

Macrovascular and tissue-level changes after stroke

The majority of stroke survivors are impaired, with nearly 33% institutionalized^{160–162} and fewer than 25% able to perform pre-stroke equivalent levels of physical activity during the six months post-stroke.¹⁶³ Only 10% of stroke patients recover completely. Thus, comprehensive systems of care are necessary which include functional mobility and cognitive rehabilitation.¹⁶⁴ No screening procedures are available in the clinic to guide patient selection for rehabilitative therapy.

Focal brain injury due to stroke affects global brain function through disruption of structural and functional connections between local and remote brain regions. Subsequent remodeling of neural networks, occurring at micro- (e.g. synaptogenesis), meso- (e.g. recruitment of accessory neuronal pathways), and macroscales (e.g. cortical remapping), may contribute to functional adaptation or compensation over time.¹⁶⁵

Yet, it remains largely unknown how specific plasticity processes contribute to functional improvement, and to what degree brain adaptations could be modulated to promote functional recovery. Various therapeutic approaches to improve neurorehabilitation have been suggested, including administration of growth-promoting drugs and stem cells,¹⁶⁶ and non-invasive brain stimulation,¹⁶⁷ but so far none of these have been effectively incorporated into standard clinical practice. It is also likely that more comprehensive surveillance of stroke survivors is required, as summarized in a recent article outlining likely requirements of impactful neural rehabilitative trials post-stroke.¹⁶⁸

Imaging enables measurement of long-term spontaneous or treatment-induced alterations in brain structure and function during recovery from stroke. Functional MRI studies in patients and animal models have demonstrated that functional recovery is associated with preservation or reinstatement of perilesional activity and interhemispheric connectivity within intact networks.^{169–171} Additionally, diffusion tensor imaging (DTI) studies have shown that functional outcome is linked to the structural integrity of remaining neuronal tracts.^{169,171} These imaging methods may therefore contribute to outcome prediction, therapy selection, and treatment monitoring in recovering stroke patients.

Neuronal excitability is mediated by glutamate and γ -aminobutyric acid (GABA), the primary excitatory and inhibitory neurotransmitters in adult brain, respectively.^{172,173} In AIS, extracellular GABA may increase, resulting in increased tonic inhibition and excitability thresholds.^{174,175} This increase in tonic inhibition is likely a safety mechanism imposed by the brain as a means to minimize neuronal damage during the initial stroke. However, as this increase in inhibition persists through sub-acute and chronic stages, it influences long-term potentiation and depression and hinders plasticity, or cognitive remapping. If the neurochemical environment can be modulated, spared peri-infarct tissue offers increased potential for plasticity. Adjuvant therapeutic modulation of excitability in both hemispheres has been shown to enhance recovery following stroke through both upregulation of excitability in the lesioned hemisphere^{176,177} and downregulation of excitability in the intact hemisphere^{178,179} using transcranial magnetic stimulation (TMS) or transcranial direct-current stimulation (tDCS). Recent work has also demonstrated recovery effects following pharmacological manipulation of tonic inhibition post-stroke.^{174,180,181} However, fundamental gaps in our knowledge persist regarding optimized implementation of these therapies and details of the physiological changes they elicit.¹⁸² Due to the biphasic role of GABA following stroke, it is likely that a subgroup of patients will benefit from dampening of

GABAergic inhibition, whereas this dampening may be harmful to patients in whom the inhibition is protective. Unfortunately, there is no consensus regarding an effective primary outcome measure in randomized controlled trials for addressing these questions.¹⁸³ The development and evaluation of novel rehabilitation strategies would be accelerated with a noninvasive imaging test to measure plasticity potential.

Neuronal and hemodynamic reorganization have been reported to occur over different anatomical scales during motor recovery: local rearrangement within primary motor cortex, increased activity in ipsilesional non-primary sensorimotor areas, and increased activity in the uninjured hemisphere.¹⁸⁴ Therefore, methods that are able to measure an array of changes to tissue physiology, over a broad spatial scale, are needed. More specifically, following stroke, corticospinal tract damage is a well-known predictor of poorer functional outcomes,¹⁸⁵ and by incorporating additional measures of excitability in ipsilesional motor cortex and interhemispheric functional connectivity, it has been reported that as much as 81% of variance in motor performance can be explained.¹⁸⁶ Furthermore, in a small cohort of patients, it has very recently been suggested that the degree of cortical inhibition within a voxel may predict response to tDCS therapy.¹⁸⁷ Therefore, multi-modal neuroimaging measurements of tissue structure and function have been suggested to have relevance for both predicting functional outcomes after stroke, as well as for predicting treatment efficacy. These studies suggest that inter-individual differences in response to intervention arise from individual factors that determine susceptibility to plasticity-inducing therapy. Individualized imaging biomarkers are needed to help stratify patients according to treatment responsiveness.

Post-stroke therapeutic interventions

A number of potential avenues for post-stroke therapy are currently being explored. The rationale for adjunctive therapies stems from the widely held theory that the functional benefits of physiotherapy are largely mediated via a combination of functional and structural plastic brain changes. Interventions that can be demonstrated to modulate brain plasticity, from pharmacological interventions to non-invasive brain stimulation (NIBS), have therefore largely been developed from the context of plasticity-inducing protocols in animal models or in healthy controls. This approach brings with it a number of important factors to consider, however, when developing successful therapies for patients: (1) it is plausible that long-term plastic changes will only be induced by multiple sessions, and (2) these therapies are unlikely

to cause a functional improvement when applied on their own, but rather require combined use with physiotherapy.¹⁸⁸

Few putative therapies have been translated into clinical trials. This so-called translational road block¹⁸⁹ has arisen for a number of reasons, including the need to extrapolate approaches from animal models, to optimize parameters for pharmacological or stimulation interventions, and to identify patients most likely to respond to a given therapy. The large size of randomized control trials needed to adequately power studies to investigate the effects of adjunctive therapies, where multicenter trials would be required to overcome the noise imparted by the inherent heterogeneity of patient populations, has to date largely proved an insurmountable obstacle.

Despite this challenge, some pharmacological interventions, particularly the selective serotonin-reuptake inhibitors (SSRIs) such as fluoxetine, and NIBS techniques such as TMS and tDCS have shown promise in proof-of-principle studies. The SSRI fluoxetine has been shown to improve functional recovery in stroke patients even in the absence of depressive symptoms,^{190,191} though it is not used routinely in clinical practice. NIBS approaches, and in particular tDCS, have also been demonstrated to lead to significant long-term clinical improvements. Anodal tDCS to the ipsilesional motor cortex^{192,193} and bilateral tDCS, where the anode is placed over the ipsilesional M1

and the cathode over the contralateral M1^{194,195} show particular promise, though the evidence for their use is still from small studies and requires further, large-scale, testing.¹⁹⁶

Future directions

Promising adjunct neurotherapies are being developed, but there is an urgent need for large-scale clinical trials to test their effectiveness. There is also a need to develop predictive markers of response to therapy, be these clinical, physiological, or imaging-based, so that patients can be given the most appropriate therapeutic intervention, thereby optimizing outcomes.

The imaging approaches outlined in the prior two sections are largely relevant for monitoring and evaluating post-stroke plasticity mechanisms, and can also be supplemented with quantitative spectroscopic imaging of GABA and glutamate, respectively. More specifically, fMRI, which most commonly exploits BOLD contrast,¹⁹⁷ is the most popular method for measuring brain function. However, BOLD signal is only an indirect and relative marker of neuronal activity, arising from complex neurochemical, metabolic, and hemodynamic modulations.^{197–199} Limited data are available on how BOLD signals relate to neurochemistry, which is likely relevant to plasticity studies. Alternative fMRI approaches sensitive to individual hemodynamic parameters, e.g. CBF, can be applied for more

Table 3. Recommended relevant research directions in the setting of cerebrovascular disease.

Population	Relevant future research direction
Moyamoya disease and syndrome	Utilizing hemodynamic imaging to monitor patients with non-atherosclerotic stenocclusive disease following revascularization procedures
Intracranial stenosis	Evaluating the role and value of cerebrovascular reserve imaging in extra- and intracranial atherosclerosis and Moyamoya disease
Sickle cell anemia	Utilizing personalized hemodynamic and metabolic signatures to identify adult patients with sickle cell anemia who require chronic transfusion therapy or other aggressive therapies vs. hydroxyurea
Small vessel disease	Further standardization of the various MRI markers of cerebral small vessel disease to develop quantitative markers that can predict changes over time
Acute ischemic and hemorrhagic stroke	Leveraging the potential of serial or longitudinal quantitative imaging, amassing big data to answer leading questions
Acute ischemic stroke	Improving precision medicine of collateral circulation in the brain by establishing a systematic framework to characterize and differentiate individual treatment based on collaterals
Acute ischemic stroke	Developing and validating novel, rapid imaging biomarkers to better understand changes in tissue metabolism in acute stroke, guiding the development of novel treatments and to aid clinical management in patients presenting outside of current treatment windows
Stroke recovery	Utilizing quantitative multi-modal imaging in the setting of post-stroke plasticity and therapy studies to identify plasticity mechanisms and also stratify patients for plasticity-inducing therapies in large clinical trials

comprehensive investigations,²⁰⁰ and such methods can be used to disambiguate absent BOLD responses in motor cortices of patients successfully performing motor tasks but with disrupted neurovascular coupling after stroke.²⁰¹ Additionally, using ¹H magnetic resonance spectroscopy (MRS) and spectral editing,^{202–204} it is possible to measure GABA and glutamate.²⁰⁵ In recent independent studies, GABA has been shown to correlate inversely with the BOLD response in human visual cortex²⁰⁶ and rat somatosensory cortex,²⁰⁷ and directly with negative BOLD responses in anterior cingulate cortex.²⁰⁸ A limitation of MRS in stroke research is its poor spatial coverage, prohibiting comparison between affected and intact tissue. Feasibility of GABA MR spectroscopic imaging (MRSI) for regional GABA quantitation has been demonstrated²⁰⁹; GABA MRSI could be well-suited to study regional differences in GABA post-stroke, but has not yet been implemented widely in patients. Newer developments that increase spatial coverage and reduce scan times hold promise.²¹⁰

Concluding remarks and future directions

This document is intended to highlight major advancements in different stages of stroke research, as well as to highlight current unmet clinical needs and future directions. Given the rapid advancement of neuroimaging methods for visualizing known physiological stroke risk factors, a major area of CVD research over the next decade will likely focus on stratification of patients for personalized therapies. As outlined above, this will likely span the spectrum of CVD and include identifying inadequate hemo-metabolic compensation mechanisms in patients with chronic arterial steno-occlusive disease, identifying collateralization extent and the ischemic penumbra in patients with acute stroke, and utilizing neuroimaging to monitor patients post-stroke and even titrate therapies based on individual potential for plasticity-inducing therapies. Realizing these goals will require coordinated efforts between the clinicians who actively manage such patients (e.g. neurologists, cardiologists, neurosurgeons, and therapists) and imaging specialists (e.g. radiologists and imaging physicists) who can develop and implement appropriate measurement tools. Relevant research areas that have been suggested by the panel of authors are highlighted in Table 3. It should also be noted that several important areas of CVD have not been covered in this consensus statement due to space restrictions, including neonatal stroke,²¹¹ small vessel disease,^{62,63} inflammation,²¹² cervical dissection,²¹³ cerebral aneurysms,²¹⁴ cardiovascular risk factors,¹⁷ and neural repair mechanisms,¹⁶⁸ however

much of the above summary is relevant to these conditions as well, and the above citations and references therein highlight these areas in more detail for the interested reader.

Funding

The author(s) disclosed receipt of the following financial support for the research, authorship, and/or publication of this article: MJD is supported by the American Heart Association (14CSA20380466 and 14GRNT20150004), NIH/NINDS (5R01NS078828, 1R01NS097763), and NIH/NINR (6R01NR015079). F-EdL is supported by a clinical established investigator grant of the Dutch Heart Foundation (grant number 2014 T060) and by a VIDi innovational grant from The Netherlands Organisation for Health Research and Development (ZonMw grant 016.126.351). MAI is funded through the Netherlands Heart Foundation (2012T008). TWO is supported by the Royal Academy of Engineering. JH has received funding from the European Research Council under the European Union's Horizon 2020 Programme (H2020)/ERC grant agreement n°637024 (HEARTOFSTROKE), H2020 grant agreement No 666881, SVDs@target and receives salary support by from the Netherlands Organization for Scientific Research (NWO) under grant n°91712322.

Declaration of conflicting interests

The author(s) declared the following potential conflicts of interest with respect to the research, authorship, and/or publication of this article: OW is the co-inventor of a patent on Delay-compensated calculation of tissue blood flow, US Patent 7,512,435, 31 March 2009, and the patent has been licensed to General Electric, Siemens, Imaging Biometrics and Olea Medical. TWO is an author on a US patent application relating to the analysis of vessel-encoded ASL data.

References

1. Feigin VL. Stroke epidemiology in the developing world. *Lancet* 2005; 365: 2160–2161.
2. Feigin V and Hoorn SV. How to study stroke incidence. *Lancet* 2004; 363: 1920–1921.
3. Bos MJ, Koudstaal PJ, Hofman A, et al. Modifiable etiological factors and the burden of stroke from the Rotterdam study: a population-based cohort study. *PLoS Med* 2014; 11: e1001634.
4. Mergenthaler P, Lindauer U, Dienel GA, et al. Sugar for the brain: the role of glucose in physiological and pathological brain function. *Trends Neurosci* 2013; 36: 587–597.
5. van Gelder NM. Brain taurine content as a function of cerebral metabolic rate: osmotic regulation of glucose derived water production. *Neurochem Res* 1989; 14: 495–497.
6. Sokoloff L. Sites and mechanisms of function-related changes in energy metabolism in the nervous system. *Dev Neurosci* 1993; 15: 194–206.
7. Martin WR, Baker RP, Grubb RL, et al. Cerebral blood volume, blood flow, and oxygen metabolism in cerebral ischaemia and subarachnoid haemorrhage: an in-vivo

- study using positron emission tomography. *Acta Neurochir* 1984; 70: 3–9.
8. Rapela CE and Green HD. Autoregulation of canine cerebral blood flow. *Circ Res* 1964; 15(Suppl): 205–212.
 9. Zaharchuk G, Mandeville JB, Bogdanov AA Jr., et al. Cerebrovascular dynamics of autoregulation and hypoperfusion. An MRI study of CBF and changes in total and microvascular cerebral blood volume during hemorrhagic hypotension. *Stroke* 1999; 30: 2197–2204; discussion 2204–2195.
 10. Prohovnik I, Hurllet-Jensen A, Adams R, et al. Hemodynamic etiology of elevated flow velocity and stroke in sickle-cell disease. *J Cereb Blood Flow Metab* 2009; 29: 803–810.
 11. Derdeyn CP, Videen TO, Yundt KD, et al. Variability of cerebral blood volume and oxygen extraction: stages of cerebral haemodynamic impairment revisited. *Brain* 2002; 125: 595–607.
 12. Powers WJ. Cerebral hemodynamics in ischemic cerebrovascular disease. *Ann Neurol* 1991; 29: 231–240.
 13. Derdeyn CP, Grubb RL Jr and Powers WJ. Cerebral hemodynamic impairment: methods of measurement and association with stroke risk. *Neurology* 1999; 53: 251–259.
 14. Derdeyn CP, Videen TO, Grubb RL Jr., et al. Comparison of PET oxygen extraction fraction methods for the prediction of stroke risk. *J Nucl Med* 2001; 42: 1195–1197.
 15. Derdeyn CP, Videen TO, Yundt KD, et al. Variability of cerebral blood volume and oxygen extraction: stages of cerebral haemodynamic impairment revisited. *Brain* 2002; 125: 595–607.
 16. Rothman KJ and Greenland S. *Modern epidemiology*. 2nd ed. Philadelphia: Lippincott-Raven, 1998.
 17. Gladstone DJ, Spring M, Dorian P, et al. Atrial fibrillation in patients with cryptogenic stroke. *N Engl J Med* 2014; 370: 2467–2477.
 18. North American Symptomatic Carotid Endarterectomy Trial (NASCET) investigators. Clinical alert: benefit of carotid endarterectomy for patients with high-grade stenosis of the internal carotid artery. National Institute of Neurological Disorders and Stroke Stroke and Trauma Division. *Stroke* 1991; 22: 816–817.
 19. North American Symptomatic Carotid Endarterectomy Trial C. Beneficial effect of carotid endarterectomy in symptomatic patients with high-grade carotid stenosis. *New Engl J Med* 1991; 325: 445–453.
 20. Kasner SE and Gorelick PB. *Prevention and treatment of ischemic stroke*. Philadelphia: Butterworth-Heinemann, 2004.
 21. Ovbiagele B, Cruz-Flores S, Lynn MJ, et al. Early stroke risk after transient ischemic attack among individuals with symptomatic intracranial artery stenosis. *Arch Neurol* 2008; 65: 733–737.
 22. Famakin BM, Chimowitz MI, Lynn MJ, et al. Causes and severity of ischemic stroke in patients with symptomatic intracranial arterial stenosis. *Stroke* 2009; 40: 1999–2003.
 23. Liebeskind DS, Cotsonis GA, Saver JL, et al. Collaterals dramatically alter stroke risk in intracranial atherosclerosis. *Ann Neurol* 2011; 69: 963–974.
 24. Zaidat OO, Fitzsimmons BF, Woodward BK, et al. Effect of a balloon-expandable intracranial stent vs medical therapy on risk of stroke in patients with symptomatic intracranial stenosis: the VISSIT randomized clinical trial. *JAMA* 2015; 313: 1240–1248.
 25. Chimowitz MI, Lynn MJ, Derdeyn CP, et al. Stenting versus aggressive medical therapy for intracranial arterial stenosis. *New Engl J Med* 2011; 365: 993–1003.
 26. Derdeyn CP, Chimowitz MI, Lynn MJ, et al. Aggressive medical treatment with or without stenting in high-risk patients with intracranial artery stenosis (SAMMPRIS): the final results of a randomised trial. *Lancet* 2014; 383: 333–341.
 27. Waters MF, Hoh BL, Lynn MJ, et al. Factors associated with recurrent ischemic stroke in the medical group of the SAMMPRIS trial. *JAMA Neurol* 2016; 73: 308–315.
 28. Mandell DM, Mossa-Basha M, Qiao Y, et al. Intracranial vessel wall MRI: Principles and expert consensus recommendations of the American Society of Neuroradiology. *Am J Neuroradiol* 2017; 38: 218–229.
 29. Scott RM and Smith ER. Moyamoya disease and moyamoya syndrome. *New Engl J Med* 2009; 360: 1226–1237.
 30. Hallemeier CL, Rich KM, Grubb RL Jr., et al. Clinical features and outcome in North American adults with moyamoya phenomenon. *Stroke* 2006; 37: 1490–1496.
 31. Kassim AA and DeBaun MR. Sickle cell disease, vasculopathy, and therapeutics. *Annu Rev Med* 2013; 64: 451–466.
 32. Phi JH, Wang KC, Lee JY, et al. Moyamoya syndrome: A window of moyamoya disease. *J Korean Neurosurg Soc* 2015; 57: 408–414.
 33. Herve D, Philippi A, Belbouab R, et al. Loss of alpha1-beta1 soluble guanylate cyclase, the major nitric oxide receptor, leads to moyamoya and achalasia. *Am J Hum Genet* 2014; 94: 385–394.
 34. Guey S, Tournier-Lasserre E, Herve D, et al. Moyamoya disease and syndromes: from genetics to clinical management. *Appl Clin Genet* 2015; 8: 49–68.
 35. Achrol AS, Guzman R, Lee M, et al. Pathophysiology and genetic factors in moyamoya disease. *Neurosurg focus* 2009; 26: E4.
 36. Scott RM, Smith JL, Robertson RL, et al. Long-term outcome in children with moyamoya syndrome after cranial revascularization by pial synangiosis. *J Neurosurg* 2004; 100: 142–149.
 37. Scott RM. Moyamoya syndrome: a surgically treatable cause of stroke in the pediatric patient. *Clin Neurosurg* 2000; 47: 378–384.
 38. Ikezaki K. Rational approach to treatment of moyamoya disease in childhood. *J Child Neurol* 2000; 15: 350–356.
 39. Kang KH, Kim HS and Kim SY. Quantitative cerebrovascular reserve measured by acetazolamide-challenged dynamic CT perfusion in ischemic adult Moyamoya disease: initial experience with angiographic correlation. *Am J Neuroradiol* 2008; 29: 1487–1493.
 40. Kawashima M, Noguchi T, Takase Y, et al. Unilateral hemispheric proliferation of ivy sign on fluid-attenuated inversion recovery images in moyamoya disease correlates highly with ipsilateral hemispheric decrease of

- cerebrovascular reserve. *Am J Neuroradiol* 2009; 30: 1709–1716.
41. Strother MK, Anderson MD, Singer RJ, et al. Cerebrovascular collaterals correlate with disease severity in adult North American patients with Moyamoya disease. *Am J Neuroradiol* 2014; 35: 1318–1324.
 42. Ni WW, Christen T, Rosenberg J, et al. Imaging of cerebrovascular reserve and oxygenation in Moyamoya disease. *J Cereb Blood Flow Metab* 2017; 37: 1213–1222.
 43. Bernaudin F, Verlhac S, Arnaud C, et al. Impact of early transcranial Doppler screening and intensive therapy on cerebral vasculopathy outcome in a newborn sickle cell anemia cohort. *Blood* 2011; 117: 1130–1140; quiz 1436.
 44. Glauser TA, Siegel MJ, Lee BC, et al. Accuracy of neurological examination and history in detecting evidence of MRI-diagnosed cerebral infarctions in children with sickle cell hemoglobinopathy. *J Child Neurol* 1995; 10: 88–92.
 45. Roach ES, Golomb MR, Adams R, et al. Management of stroke in infants and children: a scientific statement from a Special Writing Group of the American Heart Association Stroke Council and the Council on Cardiovascular Disease in the Young. *Stroke* 2008; 39: 2644–2691.
 46. Kernan WN, Ovbiagele B, Black HR, et al. Guidelines for the prevention of stroke in patients with stroke and transient ischemic attack: a guideline for healthcare professionals from the American Heart Association/American Stroke Association. *Stroke* 2014; 45: 2160–2236.
 47. Bernaudin F, Verlhac S and Chevret S. Treating sickle cell anaemia: the TWiTCH trial. *Lancet* 2016; 388: 960.
 48. Hulbert ML, McKinstry RC, Lacey JL, et al. Silent cerebral infarcts occur despite regular blood transfusion therapy after first strokes in children with sickle cell disease. *Blood* 2011; 117: 772–779.
 49. DeBaun MR, Gordon M, McKinstry RC, et al. Controlled trial of transfusions for silent cerebral infarcts in sickle cell anemia. *New Engl J Med* 2014; 371: 699–710.
 50. Watchmaker JM, Juttukonda MR, Davis LT, et al. Hemodynamic mechanisms underlying elevated oxygen extraction fraction (OEF) in moyamoya and sickle cell anemia patients. *J Cereb Blood Flow Metab*. E-pub ahead of print 2016. DOI: 271678X16682509.
 51. Bush AM, Borzage MT, Choi S, et al. Determinants of resting cerebral blood flow in sickle cell disease. *Am J Hematol* 2016; 91: 912–917.
 52. Jordan LC, Gindville MC, Scott AO, et al. Non-invasive imaging of oxygen extraction fraction in adults with sickle cell anaemia. *Brain* 2016; 139: 738–750.
 53. Bos D, Leening MJ, Kavousi M, et al. Comparison of atherosclerotic calcification in major vessel beds on the risk of all-cause and cause-specific mortality: The Rotterdam study. *Circulation. Cardiovascular imaging* 2015; 8: e003843.
 54. Bos D, Portegies ML, van der Lugt A, et al. Intracranial carotid artery atherosclerosis and the risk of stroke in whites: the Rotterdam Study. *JAMA Neurol* 2014; 71: 405–411.
 55. Lenck S, Labeyrie MA, Saint-Maurice JP, et al. Diaphragms of the carotid and vertebral arteries: an under-diagnosed cause of ischaemic stroke. *Eur J Neurol* 2014; 21: 586–593.
 56. Adams HP Jr., Bendixen BH, Kappelle LJ, et al. Classification of subtype of acute ischemic stroke. Definitions for use in a multicenter clinical trial. TOAST. Trial of Org 10172 in Acute Stroke Treatment. *Stroke* 1993; 24: 35–41.
 57. O'Donnell MJ, Chin SL, Rangarajan S, et al. Global and regional effects of potentially modifiable risk factors associated with acute stroke in 32 countries (INTERSTROKE): a case-control study. *Lancet* 2016; 388: 761–775.
 58. Bogiatzi C, Wannarong T, McLeod AI, et al. SPARKLE (Subtypes of Ischaemic Stroke Classification System), incorporating measurement of carotid plaque burden: a new validated tool for the classification of ischemic stroke subtypes. *Neuroepidemiology* 2014; 42: 243–251.
 59. Arsava EM, Ballabio E, Benner T, et al. The Causative Classification of Stroke system: an international reliability and optimization study. *Neurology* 2010; 75: 1277–1284.
 60. Wolf ME, Sauer T, Kern R, et al. Multiple subcortical acute ischemic lesions reflect small vessel disease rather than cardiogenic embolism. *J Neurol* 2012; 259: 1951–1957.
 61. De Guio F, Jouvent E, Biessels GJ, et al. Reproducibility and variability of quantitative magnetic resonance imaging markers in cerebral small vessel disease. *J Cereb Blood Flow Metab* 2016; 36: 1319–1337.
 62. Rosenberg GA, Wallin A, Wardlaw JM, et al. Consensus statement for diagnosis of subcortical small vessel disease. *J Cereb Blood Flow Metab* 2016; 36: 6–25.
 63. Wardlaw JM, Smith EE, Biessels GJ, et al. Neuroimaging standards for research into small vessel disease and its contribution to ageing and neurodegeneration. *Lancet Neurol* 2013; 12: 822–838.
 64. Werner P, Saur D, Zeisig V, et al. Simultaneous PET/MRI in stroke: a case series. *J Cereb Blood Flow Metab* 2015; 35: 1421–1425.
 65. Powers WJ, Clarke WR, Grubb RL Jr., et al. Extracranial-intracranial bypass surgery for stroke prevention in hemodynamic cerebral ischemia: the Carotid Occlusion Surgery Study randomized trial. *JAMA* 2011; 306: 1983–1992.
 66. Carlson AP, Yonas H, Chang YF, et al. Failure of cerebral hemodynamic selection in general or of specific positron emission tomography methodology?: Carotid Occlusion Surgery Study (COSS). *Stroke* 2011; 42: 3637–3639.
 67. Ribeiro MJ, Vercouillie J, Debiais S, et al. Could (18) F-DPA-714 PET imaging be interesting to use in the early post-stroke period? *EJNMMI Res* 2014; 4: 28.
 68. Dieleman N, van der Kolk AG, Zwanenburg JJ, et al. Imaging intracranial vessel wall pathology with magnetic resonance imaging: current prospects and future directions. *Circulation* 2014; 130: 192–201.
 69. Donahue MJ, Juttukonda MR and Watchmaker JM. Noise concerns and post-processing procedures in

- cerebral blood flow (CBF) and cerebral blood volume (CBV) functional magnetic resonance imaging. *NeuroImage* 2017; 154: 43–58.
70. Rapacchi S, Han F, Natsuaki Y, et al. High spatial and temporal resolution dynamic contrast-enhanced magnetic resonance angiography using compressed sensing with magnitude image subtraction. *Magn Reson Med* 2014; 71: 1771–1783.
 71. Lustig M, Donoho D and Pauly JM. Sparse MRI: The application of compressed sensing for rapid MR imaging. *Magn Reson Med* 2007; 58: 1182–1195.
 72. Lee GR, Seiberlich N, Sunshine JL, et al. Rapid time-resolved magnetic resonance angiography via a multiecho radial trajectory and GraDeS reconstruction. *Magn Reson Med* 2013; 69: 346–359.
 73. Okell TW, Schmitt P, Bi X, et al. Optimization of 4D vessel-selective arterial spin labeling angiography using balanced steady-state free precession and vessel-encoding. *NMR Biomed* 2016; 29: 776–786.
 74. Jensen-Kondering U, Lindner T, van Osch MJ, et al. Superselective pseudo-continuous arterial spin labeling angiography. *Eur J Radiol* 2015; 84: 1758–1767.
 75. Robson PM, Dai W, Shankaranarayanan A, et al. Time-resolved vessel-selective digital subtraction MR angiography of the cerebral vasculature with arterial spin labeling. *Radiology* 2010; 257: 507–515.
 76. Hendrikse J, Lu H, van der Grond J, et al. Measurements of cerebral perfusion and arterial hemodynamics during visual stimulation using TURBO-TILT. *Magn Reson Med* 2003; 50: 429–433.
 77. Wong EC. Vessel-encoded arterial spin-labeling using pseudocontinuous tagging. *Magn Reson Med* 2007; 58: 1086–1091.
 78. Okell TW, Chappell MA, Kelly ME, et al. Cerebral blood flow quantification using vessel-encoded arterial spin labeling. *J Cereb Blood Flow Metab* 2013; 33: 1716–1724.
 79. Alsop DC, Detre JA, Golay X, et al. Recommended implementation of arterial spin-labeled perfusion MRI for clinical applications: A consensus of the ISMRM perfusion study group and the European consortium for ASL in dementia. *Magn Reson Med* 2015; 73: 102–116.
 80. Schmid S, Heijtel DF, Mutsaerts HJ, et al. Comparison of velocity- and acceleration-selective arterial spin labeling with [¹⁵O]H₂O positron emission tomography. *J Cereb Blood Flow Metab* 2015; 35: 1296–1303.
 81. Wong EC, Cronin M, Wu WC, et al. Velocity-selective arterial spin labeling. *Magn Reson Med* 2006; 55: 1334–1341.
 82. Qiu D, Straka M, Zun Z, et al. CBF measurements using multidelayer pseudocontinuous and velocity-selective arterial spin labeling in patients with long arterial transit delays: comparison with xenon CT CBF. *J Magn Reson Imag* 2012; 36: 110–119.
 83. Zaharchuk G, Do HM, Marks MP, et al. Arterial spin-labeling MRI can identify the presence and intensity of collateral perfusion in patients with moyamoya disease. *Stroke* 2011; 42: 2485–2491.
 84. Qin Q and van Zijl PC. Velocity-selective-inversion prepared arterial spin labeling. *Magn Reson Med* 2016; 76: 1136–1148.
 85. Christensen S, Mouridsen K, Wu O, et al. Comparison of 10 perfusion MRI parameters in 97 sub-6-hour stroke patients using voxel-based receiver operating characteristics analysis. *Stroke* 2009; 40: 2055–2061.
 86. Donahue MJ, Faraco CC, Strother MK, et al. Bolus arrival time and cerebral blood flow responses to hypercarbia. *J Cereb Blood Flow Metab* 2014; 34: 1243–1252.
 87. MacIntosh BJ, Filippini N, Chappell MA, et al. Assessment of arterial arrival times derived from multiple inversion time pulsed arterial spin labeling MRI. *Magn Reson Med* 2010; 63: 641–647.
 88. Teeuwisse WM, Schmid S, Ghariq E, et al. Time-encoded pseudocontinuous arterial spin labeling: basic properties and timing strategies for human applications. *Magn Reson Med* 2014; 72: 1712–1722.
 89. Wells JA, Lythgoe MF, Gadian DG, et al. In vivo Hadamard encoded continuous arterial spin labeling (H-CASL). *Magn Reson Med* 2010; 63: 1111–1118.
 90. Ostergaard L, Jespersen SN, Mouridsen K, et al. The role of the cerebral capillaries in acute ischemic stroke: the extended penumbra model. *J Cereb Blood Flow Metab* 2013; 33: 635–648.
 91. Mouridsen K, Hansen MB, Ostergaard L, et al. Reliable estimation of capillary transit time distributions using DSC-MRI. *J Cereb Blood Flow Metab* 2014; 34: 1511–1521.
 92. Emblem KE, Mouridsen K, Bjornerud A, et al. Vessel architectural imaging identifies cancer patient responders to anti-angiogenic therapy. *Nat Med* 2013; 19: 1178–1183.
 93. Lemasson B, Pannetier N, Coquery N, et al. MR vascular fingerprinting in stroke and brain tumors models. *Sci Rep* 2016; 6: 37071.
 94. Su P, Mao D, Liu P, et al. Multiparametric estimation of brain hemodynamics with MR fingerprinting ASL. *Magn Reson Med*. E-pub ahead of print 26 December 2016. DOI: 10.1002/mrm.26587.
 95. Christen T, Pannetier NA, Ni WW, et al. MR vascular fingerprinting: A new approach to compute cerebral blood volume, mean vessel radius, and oxygenation maps in the human brain. *NeuroImage* 2014; 89: 262–270.
 96. Wells JA, Thomas DL, Saga T, et al. MRI of cerebral micro-vascular flow patterns: A multi-direction diffusion-weighted ASL approach. *J Cereb Blood Flow Metab* 2017; 37: 2076–2083.
 97. van der Kolk AG, Zwanenburg JJ, Brundel M, et al. Intracranial vessel wall imaging at 7.0-T MRI. *Stroke* 2011; 42: 2478–2484.
 98. Connolly ES Jr., Rabinstein AA, Carhuapoma JR, et al. Guidelines for the management of aneurysmal subarachnoid hemorrhage: a guideline for healthcare professionals from the American Heart Association/American Stroke Association. *Stroke* 2012; 43: 1711–1737.
 99. O’Kelly CJ, Kulkarni AV, Austin PC, et al. The impact of therapeutic modality on outcomes following repair of ruptured intracranial aneurysms: an administrative data analysis. Clinical article. *J Neurosurg* 2010; 113: 795–801.
 100. Rincon F and Mayer SA. The epidemiology of intracerebral hemorrhage in the United States from 1979 to 2008. *Neurocrit Care* 2013; 19: 95–102.

101. Hemphill JC III, Greenberg SM, Anderson CS, et al. Guidelines for the management of spontaneous intracerebral hemorrhage: A guideline for healthcare professionals from the American Heart Association/American Stroke Association. *Stroke* 2015; 46: 2032–2060.
102. Delgado Almandoz JE, Yoo AJ, Stone MJ, et al. The spot sign score in primary intracerebral hemorrhage identifies patients at highest risk of in-hospital mortality and poor outcome among survivors. *Stroke* 2010; 41: 54–60.
103. Brouwers HB, Battey TW, Musial HH, et al. Rate of contrast extravasation on computed tomographic angiography predicts hematoma expansion and mortality in primary intracerebral hemorrhage. *Stroke* 2015; 46: 2498–2503.
104. Le TT, Fischbein NJ, Andre JB, et al. Identification of venous signal on arterial spin labeling improves diagnosis of dural arteriovenous fistulas and small arteriovenous malformations. *Am J Neuroradiol* 2012; 33: 61–68.
105. Hodel J, Leclerc X, Kalsoum E, et al. Intracranial arteriovenous shunting: Detection with arterial spin-labeling and susceptibility-weighted imaging combined. *Am J Neuroradiol* 2017; 38: 71–76.
106. Yamamoto N, Satomi J, Yamamoto Y, et al. Usefulness of 3-Tesla magnetic resonance arterial spin-labeled imaging for diagnosis of cranial dural arteriovenous fistula. *J Neurol Sci* 2017; 372: 428–432.
107. Mozaffarian D, Benjamin EJ, Go AS, et al. Heart disease and stroke statistics—2015 update: a report from the American Heart Association. *Circulation* 2015; 131: e29–e322.
108. Group TNiONDaSr-PSS. Tissue plasminogen activator for acute ischemic stroke. The National Institute of Neurological Disorders and Stroke rt-PA Stroke Study Group. *New Engl J Med* 1995; 333: 1581–1587.
109. Heit JJ and Wintermark M. Imaging selection for reperfusion therapy in acute ischemic stroke. *Curr Treat Options Neurol* 2015; 17: 332.
110. Berkhemer OA, Fransen PS, Beumer D, et al. A randomized trial of intraarterial treatment for acute ischemic stroke. *New Engl J Med* 2015; 372: 11–20.
111. Jovin TG, Chamorro A, Cobo E, et al. Thrombectomy within 8 hours after symptom onset in ischemic stroke. *New Engl J Med* 2015; 372: 2296–2306.
112. Campbell BC, Mitchell PJ, Kleinig TJ, et al. Endovascular therapy for ischemic stroke with perfusion-imaging selection. *New Engl J Med* 2015; 372: 1009–1018.
113. Saver JL, Goyal M, Bonafe A, et al. Stent-retriever thrombectomy after intravenous t-PA vs. t-PA alone in stroke. *New Engl J Med* 2015; 372: 2285–2295.
114. Goyal M, Demchuk AM, Menon BK, et al. Randomized assessment of rapid endovascular treatment of ischemic stroke. *N Engl J Med* 2015; 372: 1019–1030.
115. Hacke W, Kaste M, Bluhmki E, et al. Thrombolysis with alteplase 3 to 4.5 hours after acute ischemic stroke. *New Engl J Med* 2008; 359: 1317–1329.
116. Wechsler LR. Intravenous thrombolytic therapy for acute ischemic stroke. *New Engl J Med* 2011; 364: 2138–2146.
117. Hesselmann V, Niederstadt T, Dziewas R, et al. Reperfusion by combined thrombolysis and mechanical thrombectomy in acute stroke: effect of collateralization, mismatch, and time to and grade of recanalization on clinical and tissue outcome. *Am J Neuroradiol* 2012; 33: 336–342.
118. Broderick JP, Palesch YY, Demchuk AM, et al. Endovascular therapy after intravenous t-PA versus t-PA alone for stroke. *New Engl J Med* 2013; 368: 893–903.
119. Fiehler J, Foth M, Kucinski T, et al. Severe ADC decreases do not predict irreversible tissue damage in humans. *Stroke* 2002; 33: 79–86.
120. Rivers CS and Wardlaw JM. What has diffusion imaging in animals told us about diffusion imaging in patients with ischaemic stroke? *Cerebrovasc Dis* 2005; 19: 328–336.
121. Parsons MW, Yang Q, Barber PA, et al. Perfusion magnetic resonance imaging maps in hyperacute stroke: relative cerebral blood flow most accurately identifies tissue destined to infarct. *Stroke* 2001; 32: 1581–1587.
122. Kamalian S, Kamalian S, Konstas AA, et al. CT perfusion mean transit time maps optimally distinguish benign oligemia from true “at-risk” ischemic penumbra, but thresholds vary by postprocessing technique. *Am J Neuroradiol* 2012; 33: 545–549.
123. Kidwell CS, Alger JR and Saver JL. Evolving paradigms in neuroimaging of the ischemic penumbra. *Stroke* 2004; 35: 2662–2665.
124. Rivers CS, Wardlaw JM, Armitage PA, et al. Do acute diffusion- and perfusion-weighted MRI lesions identify final infarct volume in ischemic stroke? *Stroke* 2006; 37: 98–104.
125. Hossmann KA. Cerebral ischemia: models, methods and outcomes. *Neuropharmacology* 2008; 55: 257–270.
126. Federau C, Sumer S, Becce F, et al. Intravoxel incoherent motion perfusion imaging in acute stroke: initial clinical experience. *Neuroradiology* 2014; 56: 629–635.
127. Lv Y, Margulies DS, Cameron Craddock R, et al. Identifying the perfusion deficit in acute stroke with resting-state functional magnetic resonance imaging. *Ann Neurol* 2013; 73: 136–140.
128. Christen T, Jahanian H, Ni WW, et al. Noncontrast mapping of arterial delay and functional connectivity using resting-state functional MRI: a study in Moyamoya patients. *J Magn Reson Imag* 2015; 41: 424–430.
129. Barber PA, Demchuk AM, Zhang J, et al. Validity and reliability of a quantitative computed tomography score in predicting outcome of hyperacute stroke before thrombolytic therapy. ASPECTS Study Group. Alberta Stroke Programme Early CT Score. *Lancet* 2000; 355: 1670–1674.
130. Warach SJ, Luby M, Albers GW, et al. Acute stroke imaging research roadmap III imaging selection and outcomes in acute stroke reperfusion clinical trials:

- Consensus recommendations and further research priorities. *Stroke* 2016; 47: 1389–1398.
131. Rebello LC, Bouslama M, Haussen DC, et al. Endovascular treatment for patients with acute stroke who have a large ischemic core and large mismatch imaging profile. *JAMA Neurol* 2017; 74: 34–40.
 132. van Seeters T, Biessels GJ, van der Schaaf IC, et al. Prediction of outcome in patients with suspected acute ischaemic stroke with CT perfusion and CT angiography: the Dutch acute stroke trial (DUST) study protocol. *BMC Neurol* 2014; 14: 37.
 133. Kidwell CS, Chalela JA, Saver JL, et al. Comparison of MRI and CT for detection of acute intracerebral hemorrhage. *JAMA* 2004; 292: 1823–1830.
 134. Wang DJ, Alger JR, Qiao JX, et al. Multi-delay multiparametric arterial spin-labeled perfusion MRI in acute ischemic stroke-Comparison with dynamic susceptibility contrast enhanced perfusion imaging. *NeuroImage Clin* 2013; 3: 1–7.
 135. Bokkers RP, Hernandez DA, Merino JG, et al. Whole-brain arterial spin labeling perfusion MRI in patients with acute stroke. *Stroke* 2012; 43: 1290–1294.
 136. Minnerup J, Broocks G, Kalkoffen J, et al. Computed tomography-based quantification of lesion water uptake identifies patients within 4.5 hours of stroke onset: A multicenter observational study. *Ann Neurol* 2016; 80: 924–934.
 137. McGarry BL, Rogers HJ, Knight MJ, et al. Stroke onset time estimation from multispectral quantitative magnetic resonance imaging in a rat model of focal permanent cerebral ischemia. *Int J Stroke* 2016; 11: 677–682.
 138. Kim SJ, Son JP, Ryoo S, et al. A novel magnetic resonance imaging approach to collateral flow imaging in ischemic stroke. *Ann Neurol* 2014; 76: 356–369.
 139. Villringer K, Serrano-Sandoval R, Grittner U, et al. Subtracted dynamic MR perfusion source images (sMRP-SI) provide collateral blood flow assessment in MCA occlusions and predict tissue fate. *Eur Radiol* 2016; 26: 1396–1403.
 140. Oja JM, Gillen JS, Kauppinen RA, et al. Determination of oxygen extraction ratios by magnetic resonance imaging. *J Cereb Blood Flow Metab* 1999; 19: 1289–1295.
 141. Wright GA, Hu BS and Macovski A. 1991 I.I. Rabi Award. Estimating oxygen saturation of blood in vivo with MR imaging at 1.5 T. *J Magn Reson Imag* 1991; 1: 275–283.
 142. An H and Lin W. Impact of intravascular signal on quantitative measures of cerebral oxygen extraction and blood volume under normo- and hypercapnic conditions using an asymmetric spin echo approach. *Magn Reson Med* 2003; 50: 708–716.
 143. Lu H and Ge Y. Quantitative evaluation of oxygenation in venous vessels using T2-relaxation-under-spin-tagging MRI. *Magn Reson Med* 2008; 60: 357–363.
 144. Xia S, Utriainen D, Tang J, et al. Decreased oxygen saturation in asymmetrically prominent cortical veins in patients with cerebral ischemic stroke. *Magn Reson Imag* 2014; 32: 1272–1276.
 145. Bolar DS, Rosen BR, Sorensen AG, et al. QUantitative Imaging of eXtraction of oxygen and TIssue consumption (QUIXOTIC) using venular-targeted velocity-selective spin labeling. *Magn Reson Med* 2011; 66: 1550–1562.
 146. Christen T, Zaharchuk G, Pannetier N, et al. Quantitative MR estimates of blood oxygenation based on T2*: a numerical study of the impact of model assumptions. *Magn Reson Med* 2012; 67: 1458–1468.
 147. Dani KA, Santosh C, Brennan D, et al. T2*-weighted magnetic resonance imaging with hyperoxia in acute ischemic stroke. *Ann Neurol* 2010; 68: 37–47.
 148. Guivel-Scharen V, Sinnwell T, Wolff SD, et al. Detection of proton chemical exchange between metabolites and water in biological tissues. *J Magn Reson* 1998; 133: 36–45.
 149. van Zijl PC and Yadav NN. Chemical exchange saturation transfer (CEST): what is in a name and what isn't? *Magn Reson Med* 2011; 65: 927–948.
 150. Zhou J, Payen J, Wilson DA, et al. Using the amide proton signals of intracellular proteins and peptides to detect pH effects in MRI. *Nature Med* 2003; 9: 1085–1090.
 151. Zhou JY and van Zijl PCM. Defining an acidosis-based ischemic penumbra from pH-weighted MRI. *Transl Stroke Res* 2012; 3: 76–83.
 152. Leigh R, Knutsson L, Zhou J, et al. Imaging the physiological evolution of the ischemic penumbra in acute ischemic stroke. *J Cereb Blood Flow Metab*. E-pub ahead of print 27 March 2017. DOI: 271678X17700913.
 153. Kakuda W, Lansberg MG, Thijs VN, et al. Optimal definition for PWI/DWI mismatch in acute ischemic stroke patients. *J Cereb Blood Flow Metab* 2008; 28: 887–891.
 154. An H, Ford AL, Chen Y, et al. Defining the ischemic penumbra using magnetic resonance oxygen metabolic index. *Stroke* 2015; 46: 982–988.
 155. Sun PZ, Zhou J, Sun W, et al. Detection of the ischemic penumbra using pH-weighted MRI. *J Cereb Blood Flow Metab* 2007; 27: 1129–1136.
 156. Harston GW, Tee YK, Blockley N, et al. Identifying the ischaemic penumbra using pH-weighted magnetic resonance imaging. *Brain* 2015; 138: 36–42.
 157. Tietze A, Blicher J, Mikkelsen IK, et al. Assessment of ischemic penumbra in patients with hyperacute stroke using amide proton transfer (APT) chemical exchange saturation transfer (CEST) MRI. *NMR Biomed* 2014; 27: 163–174.
 158. Griswold MA, Jakob PM, Heidemann RM, et al. Generalized autocalibrating partially parallel acquisitions (GRAPPA). *Magn Reson Med* 2002; 47: 1202–1210.
 159. Setsompop K, Gagoski BA, Polimeni JR, et al. Blipped-controlled aliasing in parallel imaging for simultaneous multislice echo planar imaging with reduced g-factor penalty. *Magn Reson Med* 2012; 67: 1210–1224.
 160. Ng YS, Stein J, Ning M, et al. Comparison of clinical characteristics and functional outcomes of ischemic stroke in different vascular territories. *Stroke* 2007; 38: 2309–2314.

161. Dobkin BH. Strategies for stroke rehabilitation. *Lancet Neurol* 2004; 3: 528–536.
162. Lai SM, Studenski S, Duncan PW, et al. Persisting consequences of stroke measured by the Stroke Impact Scale. *Stroke* 2002; 33: 1840–1844.
163. Duncan PW, Lai SM and Keighley J. Defining post-stroke recovery: implications for design and interpretation of drug trials. *Neuropharmacology* 2000; 39: 835–841.
164. Xie J, George MG, Ayala C, et al. Outpatient rehabilitation among stroke survivors—21 States and the District of Columbia, 2005. *MMWR Morb Mortal Wkly Rep* 2007; 56: 504–507.
165. Carmichael ST. Plasticity of cortical projections after stroke. *Neuroscientist* 2003; 9: 64–75.
166. Hermann DM and Chopp M. Promoting brain remodeling and plasticity for stroke recovery: therapeutic promise and potential pitfalls of clinical translation. *Lancet Neurol* 2012; 11: 369–380.
167. Hummel FC, Celnik P, Pascual-Leone A, et al. Controversy: Noninvasive and invasive cortical stimulation show efficacy in treating stroke patients. *Brain Stimul* 2008; 1: 370–382.
168. Dobkin BH and Carmichael ST. The specific requirements of neural repair trials for stroke. *Neurorehabil Neural Repair* 2016; 30: 470–478.
169. Dijkhuizen RM, van der Marel K, Otte WM, et al. Functional MRI and diffusion tensor imaging of brain reorganization after experimental stroke. *Transl Stroke Res* 2012; 3: 36–43.
170. Dijkhuizen RM, Zaharchuk G and Otte WM. Assessment and modulation of resting-state neural networks after stroke. *Curr Opin Neurol* 2014; 27: 637–643.
171. Grefkes C and Fink GR. Connectivity-based approaches in stroke and recovery of function. *Lancet Neurol* 2014; 13: 206–216.
172. Hyder F, Rothman DL and Bennett MR. Cortical energy demands of signaling and nonsignaling components in brain are conserved across mammalian species and activity levels. *Proc Natl Acad Sci USA* 2013; 110: 3549–3554.
173. Buzsaki G, Kaila K and Raichle M. Inhibition and brain work. *Neuron* 2007; 56: 771–783.
174. Clarkson AN, Huang BS, Macisaac SE, et al. Reducing excessive GABA-mediated tonic inhibition promotes functional recovery after stroke. *Nature* 2010; 468: 305–309.
175. Clarkson AN. Perisynaptic GABA receptors: The overzealous protector. *Adv Pharmacol Sci* 2012; 2012: 708428.
176. Hummel F, Celnik P, Giraux P, et al. Effects of non-invasive cortical stimulation on skilled motor function in chronic stroke. *Brain* 2005; 128: 490–499.
177. Hummel F and Cohen LG. Improvement of motor function with noninvasive cortical stimulation in a patient with chronic stroke. *Neurorehabil Neural Repair* 2005; 19: 14–19.
178. Plewnia C, Lotze M and Gerloff C. Disinhibition of the contralateral motor cortex by low-frequency rTMS. *Neuroreport* 2003; 14: 609–612.
179. Schambra HM, Sawaki L and Cohen LG. Modulation of excitability of human motor cortex (M1) by 1 Hz transcranial magnetic stimulation of the contralateral M1. *Clin Neurophysiol* 2003; 114: 130–133.
180. Lazar RM, Fitzsimmons BF, Marshall RS, et al. Midazolam challenge reinduces neurological deficits after transient ischemic attack. *Stroke* 2003; 34: 794–796.
181. Lazar RM, Berman MF, Festa JR, et al. GABAergic but not anti-cholinergic agents re-induce clinical deficits after stroke. *J Neurol Sci* 2010; 292: 72–76.
182. Hummel FC and Cohen LG. Non-invasive brain stimulation: a new strategy to improve neurorehabilitation after stroke? *Lancet Neurol* 2006; 5: 708–712.
183. Ali M, English C, Bernhardt J, et al. More outcomes than trials: a call for consistent data collection across stroke rehabilitation trials. *Int J Stroke* 2013; 8: 18–24.
184. Johansen-Berg H. Functional imaging of stroke recovery: what have we learnt and where do we go from here? *Int J Stroke* 2007; 2: 7–16.
185. Ward NS, Newton JM, Swayne OB, et al. Motor system activation after subcortical stroke depends on corticospinal system integrity. *Brain* 2006; 129: 809–819.
186. Volz LJ, Sarfeld AS, Diekhoff S, et al. Motor cortex excitability and connectivity in chronic stroke: a multimodal model of functional reorganization. *Brain Struct Funct* 2015; 220: 1093–1107.
187. O’Shea J, Boudrias MH, Stagg CJ, et al. Predicting behavioural response to TDCS in chronic motor stroke. *NeuroImage* 2014; 85(Pt 3): 924–933.
188. Group ATC, Bernhardt J, Langhorne P, et al. Efficacy and safety of very early mobilisation within 24 h of stroke onset (AVERT): a randomised controlled trial. *Lancet* 2015; 386: 46–55.
189. Endres M, Engelhardt B, Koistinaho J, et al. Improving outcome after stroke: overcoming the translational roadblock. *Cerebrovasc Dis* 2008; 25: 268–278.
190. Chollet F, Tardy J, Albuher J-F, et al. Fluoxetine for motor recovery after acute ischaemic stroke (FLAME): a randomised placebo-controlled trial. *Lancet Neurol* 2011; 10: 123–130.
191. Mead GE, Hsieh C-F, Lee R, et al. Selective serotonin reuptake inhibitors (SSRIs) for stroke recovery. *Cochrane Database Syst Rev (Online)* 2013; 44: 844–850.
192. Butler A, Shuster M, O’Hara E, et al. A meta-analysis of the efficacy of anodal transcranial direct current stimulation for upper limb motor recovery in stroke survivors. *J Hand Ther* 2013; 26: 162–171.
193. Allman C, Amadi U, Winkler AM, et al. Ipsilesional anodal tDCS enhances the functional benefits of rehabilitation in patients with chronic stroke. *Sci Transl Med* 2016; 8: 330re331 331–339.
194. Lindenberg R, Renga V, Zhu LL, et al. Bihemispheric brain stimulation facilitates motor recovery in chronic stroke patients. *Neurology* 2010; 75: 2176–2184.
195. Kang N, Summers JJ and Cauraugh JH. Transcranial direct current stimulation facilitates motor learning post-stroke: a systematic review and meta-analysis. *J Neurol Neurosurg Psychiatry* 2016; 87: 345–355.

196. Marquez J, van Vliet P, McElduff P, et al. Transcranial direct current stimulation (tDCS): does it have merit in stroke rehabilitation? A systematic review. *Int J Stroke* 2015; 10: 306–316.
197. Ogawa S, Lee TM, Kay AR, et al. Brain magnetic resonance imaging with contrast dependent on blood oxygenation. *Proc Natl Acad Sci USA* 1990; 87: 9868–9872.
198. Buxton RB, Uludag K, Dubowitz DJ, et al. Modeling the hemodynamic response to brain activation. *Neuroimage* 2004; 23(Suppl 1): S220–S233.
199. van Zijl PC, Eleff SM, Ulatowski JA, et al. Quantitative assessment of blood flow, blood volume and blood oxygenation effects in functional magnetic resonance imaging. *Nat Med* 1998; 4: 159–167.
200. Donahue MJ, Blicher JU, Ostergaard L, et al. Cerebral blood flow, blood volume, and oxygen metabolism dynamics in human visual and motor cortex as measured by whole-brain multi-modal magnetic resonance imaging. *J Cereb Blood Flow Metab* 2009; 29: 1856–1866.
201. Blicher JU, Stagg CJ, O’Shea J, et al. Visualization of altered neurovascular coupling in chronic stroke patients using multimodal functional MRI. *J Cereb Blood Flow Metab* 2012; 32: 2044–2054.
202. Mescher M, Merkle H, Kirsch J, et al. Simultaneous in vivo spectral editing and water suppression. *NMR Biomed* 1998; 11: 266–272.
203. Edden RA and Barker PB. Spatial effects in the detection of gamma-aminobutyric acid: improved sensitivity at high fields using inner volume saturation. *Magn Reson Med* 2007; 58: 1276–1282.
204. Waddell KW, Avison MJ, Joers JM, et al. A practical guide to robust detection of GABA in human brain by J-difference spectroscopy at 3 T using a standard volume coil. *Magn Reson Imaging* 2007; 25: 1032–1038.
205. Waddell KW, Zanjani-pour P, Pradhan S, et al. Anterior cingulate and cerebellar GABA and Glu correlations measured by (1)H J-difference spectroscopy. *Magn Reson Imaging* 2011; 29: 19–24.
206. Muthukumaraswamy SD, Edden RA, Jones DK, et al. Resting GABA concentration predicts peak gamma frequency and fMRI amplitude in response to visual stimulation in humans. *Proc Natl Acad Sci USA* 2009; 106: 8356–8361.
207. Chen Z, Silva AC, Yang J, et al. Elevated endogenous GABA level correlates with decreased fMRI signals in the rat brain during acute inhibition of GABA transaminase. *J Neurosci Res* 2005; 79: 383–391.
208. Northoff G, Walter M, Schulte RF, et al. GABA concentrations in the human anterior cingulate cortex predict negative BOLD responses in fMRI. *Nat Neurosci* 2007; 10: 1515–1517.
209. Zhu H, Edden RA, Ouwerkerk R, et al. High resolution spectroscopic imaging of GABA at 3 Tesla. *Magn Reson Med* 2011; 65: 603–609.
210. Bogner W, Gagoski B, Hess AT, et al. 3D GABA imaging with real-time motion correction, shim update and reacquisition of adiabatic spiral MRSI. *NeuroImage* 2014; 103: 290–302.
211. Lee S, Mirsky DM, Beslow LA, et al. Pathways for neuroimaging of neonatal stroke. *Pediatr Neurol* 2017; 69: 37–48.
212. Gounis MJ, van der Marel K, Marosfoi M, et al. Imaging inflammation in cerebrovascular disease. *Stroke* 2015; 46: 2991–2997.
213. Biller J, Sacco RL, Albuquerque FC, et al. Cervical arterial dissections and association with cervical manipulative therapy: a statement for healthcare professionals from the American Heart Association/American Stroke Association. *Stroke* 2014; 45: 3155–3174.
214. Chalouhi N, Hoh BL and Hasan D. Review of cerebral aneurysm formation, growth, and rupture. *Stroke* 2013; 44: 3613–3622.
215. Donahue MJ, Strother MK and Hendrikse J. Novel MRI approaches for assessing cerebral hemodynamics in ischemic cerebrovascular disease. *Stroke* 2012; 43: 903–915.
216. Donahue MJ, Dethrage LM, Faraco CC, et al. Routine clinical evaluation of cerebrovascular reserve capacity using carbogen in patients with intracranial stenosis. *Stroke* 2014; 45: 2335–2341.
217. Arteaga DF, Strother MK, Davis LT, et al. Planning-free cerebral blood flow territory mapping in patients with intracranial arterial stenosis. *J Cereb Blood Flow Metab* 2017; 37: 1944–1958.
218. Leenders KL, Perani D, Lammertsma AA, et al. Cerebral blood flow, blood volume and oxygen utilization. Normal values and effect of age. *Brain* 1990; 113(Pt 1): 27–47.
219. Mishra NK, Christensen S, Wouters A, et al. Reperfusion of very low cerebral blood volume lesion predicts parenchymal hematoma after endovascular therapy. *Stroke* 2015; 46: 1245–1249.
220. Rohl L, Ostergaard L, Simonsen CZ, et al. Viability thresholds of ischemic penumbra of hyperacute stroke defined by perfusion-weighted MRI and apparent diffusion coefficient. *Stroke* 2001; 32: 1140–1146.
221. Rottenberg DA, Ginos JZ, Kearfott KJ, et al. In vivo measurement of regional brain tissue pH using positron emission tomography. *Ann Neurol* 1984; 15(Suppl): S98–S102.
222. Hatazawa J, Fujita H, Kanno I, et al. Regional cerebral blood flow, blood volume, oxygen extraction fraction, and oxygen utilization rate in normal volunteers measured by the autoradiographic technique and the single breath inhalation method. *Ann Nucl Med* 1995; 9: 15–21.
223. Scheinberg P and Stead EA. The cerebral blood flow in male subjects as measured by the nitrous oxide technique. Normal values for blood flow, oxygen utilization, glucose utilization, and peripheral resistance, with observations on the effect of tilting and anxiety. *J Clin Invest* 1949; 28: 1163–1171.
224. Phelps ME. Positron computed tomography studies of cerebral glucose metabolism in man: theory and

- application in nuclear medicine. *Semin Nucl Med* 1981; 11: 32–49.
225. Huang SC, Phelps ME, Hoffman EJ, et al. Noninvasive determination of local cerebral metabolic rate of glucose in man. *Am J Physiol* 1980; 238: E69–E82.
226. Heiss WD, Huber M, Fink GR, et al. Progressive derangement of periinfarct viable tissue in ischemic stroke. *J Cereb Blood Flow Metab* 1992; 12: 193–203.
227. Hankey GJ. Potential new risk factors for ischemic stroke: what is their potential? *Stroke* 2006; 37: 2181–2188.
228. O'Donnell MJ, Xavier D, Liu L, et al. Risk factors for ischaemic and intracerebral haemorrhagic stroke in 22 countries (the INTERSTROKE study): a case-control study. *Lancet* 2010; 376: 112–123.